Modelling of creep compacting outcrop chalks injected with Ca-Mg-Na-Cl brines at reservoir conditions

Pål Østebø Andersen[1,2,3] and Dhruvit Satishchandra Berawala[2,3]
1 Department of Energy Resources, University of Stavanger, Norway
2 Department of Energy and Petroleum Engineering, University of Stavanger, Norway
3 The National IOR Centre of Norway, University of Stavanger, Norway

Abstract

Numerical and analytical 1D solutions are presented to interpret the link between geochemical alterations and creep compaction (compaction under constant effective stress) in chalk cores. Chemically reactive flow enhancing chalk compaction is of significant importance for EOR, compaction and subsidence in North Sea chalk reservoirs. The focus of the study is on Ca-Mg-Na-Cl brines that interact with the chalk by dissolution of calcite and precipitation of magnesite.

An explicit analytical solution is derived for the steady state ion and dissolution rate distributions at a given injected composition and injection rate. A mathematical description of creep compaction is proposed based on applied affective stresses and the rocks ability to carry that stress as function of porosity. The reaction and compaction models are then coupled as follows: The compaction rate is assumed enhanced by the dissolution rate, which can vary spatially. Further, the solid volume changes by mineral dissolution and precipitation. Brine-dependent and non-uniform compaction is hence built into the model via the dissolution rate distribution.

The model is validated and parameterized against data from a total of 22 core samples from two chalk types (Aalborg and Liege) where reactive and inert brines were injected from ambient to Ekofisk reservoir conditions (130 °C). Experimentally measured effluent concentrations, distributions in mineralogy after flooding and creep compaction behavior were matched. Our model is the first to link a vast set of data on this subject and predict performance under new experimental conditions. That also represents a first step in upscaling such results from lab towards field. Our interpretations indicate that the two chalk types would respond differently chemically and by compaction to changes in concentration and injection rate. Brines injected through Liege chalk appeared to approach stable oversaturation, while in Aalborg, the equilibrium condition was in agreement with geochemical calculations.

Key words: Chalk; chemical compaction; creep compaction; reactive flow; numerical and analytical solutions

Nomenclature

Roman:

C_i	=	Brine concentration, mol / m^3
CEC	=	Cation exchange capacity, mol / m^3
D	=	Dispersion coefficient, m^2 / s
d_c	=	Core diameter, m
f	=	Fraction of loadbearing area, -
F_m	=	Effective stress (microscopic), Pa
$\dot{r}$	=	Reaction rate, mol / m^3 / s
$\dot{r}_{ref}$	=	Tuning parameter, mol / m^3 / s
K	=	Ion exchange equilibrium constant, -
k_c	=	Stress compaction coefficient, $1/\mathrm{Pa/s}$
k_{c0}	=	Chemistry independent component of k, $1/\mathrm{Pa/s}$
k_c^{max}	=	Max compaction coefficient, 1 / Pa / s
k_1	=	Reaction rate constant, $1/\left(\frac{\mathrm{mol}}{\mathrm{m}^3}\right)^{n-1}$ /s
k_2	=	Reaction rate equilibrium constant, -

L = Core length, m
M_{wi} = Molar weight, kg/mol
n = Reaction order, -
$N_{Da,n}$ = Dahmköhler number, -
p_f = Pore fluid pressure, Pa
P_{con} = Confining pressure, Pa
R = Universal gas constant, J/mol/K
T = Absolute temperature, K
V = Volume, m^3
V_{p_r} = Pore volume reduction, -
V_{s_r} = Solid volume reduction, -
v_w = Water interstitial velocity, m/s

Greek:

β = Biot coefficient, -
β_i = Equivalent fraction, -
ϵ = Strain, -
ρ_i = Mineral concentration, mol / m^3
ρ_i^s = Surface species concentration, mol / m^3
σ = Stress (macroscopic), Pa
σ' = Effective stress (macroscopic), Pa
ϕ = Porosity, -
ω_i = Mineral density, kg / m^3

Indices:

0 = Initial state of creep
aq = Aqueous
c = Calcite
ca = Calcium
eq = Reactive equilibrium state
i = Species
inj = Injected concentration state
j = Slice (of core)
m = Magnesite
mg = Magnesium
nacl = Sodium Cloride
p = Pore
r = Radial direction
s = Solid
vol = Volumetric
x = Axial direction

Abbreviations:

EOR = Enhanced oil recovery
PV = Pore volume

Introduction

Chemically reactive flow is a key phenomenon in underground storage and transport. For the petroleum industry relevant processes range from fines migration, precipitation and scaling events, carbon capture and storage, wettability alteration, geological development of sedimentary structures and weakening of loadbearing formations (Shinn & Robbin 1983; Kharaka et al. 2006; Austad et al. 2008). Seawater injection for pressure drive oil recovery in especially chalk formations has displayed strong reactive

interaction with implications on wettability and compaction. Chalks are characterized by high porosity (~ 40 to 50 %) and permeability in mD range, but also high reactivity due to high specific surface area ~ 2 to 5 m^2/g (Hjuler 2007; Andersen et al. 2018). In the giant chalk field Ekofisk, reservoir compaction was observed during primary production. Water injection was performed, but the compaction continued even after pressure stabilization (Sylte et al. 1999). Similarly, Ruddy et al. (1989) documented compaction as a key mechanism on the Valhall chalk field. Research on core scale has demonstrated that chalk is weakened by the reactive interaction with seawater. In particular the seawater ions Mg^{2+}, SO_4^{2-} and Ca^{2+} interact with the rock in a complex interplay and lead to dissolution of the calcite mineral $CaCO_3$ (Madland et al. 2011), the main constituent in the chalk matrix. Oil recovery in chalk is strongly driven by spontaneous imbibition (Cuiec et al. 1994; Graue et al. 1999; Morrow & Mason 2001) due to the extensive fracturing often seen in carbonates and strong capillary forces in low permeable rocks (Akin et al. 2000). A high EOR potential by brine dependent spontaneous imbibition has been demonstrated for chalks by varying the ions naturally appearing in seawater (Hirasaki & Zhang 2004; Zhang et al. 2007).

To predict the outcome of changing the injected brine for EOR purposes, much focus has been dedicated towards replicating proper stress and temperature conditions as those in the field and study the chemo-mechanical behavior. This often involves loading chalk cores beyond their yield point in triaxial cells and leaving them at constant effective stress conditions while they compact with time (creep compaction (Fjær et al. 1992)). During these tests brines of various compositions are injected. The composition produced from the effluent is indicative of whether chemical interactions have taken place. Seawater and reservoir core material are often complex in composition and thus di-ionic brines and relatively pure outcrop chalks are most often studied to make reliable conclusions. The flooding-compaction processes have been shown to depend on brine composition, temperature, chalk type and non-carbonate content. With other parameters fixed, at elevated temperatures the reactivity and dissolution increases, as seen by higher net production of Ca^{2+} ions in the effluent. This correlates well with enhanced compaction. As an example, Megawati et al. (2011) demonstrated that switching from injecting reactive $MgCl_2$ brine to an inert brine reduced the compaction rate practically to zero. Switching to a reactive brine again activated compaction. Minde et al. (2018) observed that $MgCl_2$ brines injected at low temperature (ambient) were as low reactive as NaCl at high temperature (130 °C). The cores' compaction behavior was comparable. $MgCl_2$ brines injected at higher temperature lead to much higher dissolution and compaction. Further, the compaction trends with time have been shown to depend on brine and chalk type (Megawati et al. 2015; Andersen et al. 2018). Cores injected with low reactive brines tend to compact with logarithmic strain vs time profiles. The same was observed when injecting reactive $MgCl_2$ into impure chalks (containing ~5 wt % non-carbonate), but at higher compaction rates. On the other hand, injection of $MgCl_2$ into pure chalks displayed an induction time in compaction before a sudden acceleration and the more expected logarithmic trend. The acceleration of compaction was accompanied by increased dissolution.

Several mathematical models have been developed to interpret the chemical interactions taking place by coupling reaction kinetics and equilibrium chemistry with advection-dispersion models (Evje et al. 2009; Andersen et al. 2012, 2018; Andersen & Evje 2016). This has been possible by identifying some of the main mineralogical alterations taking place. During $MgCl_2$ injection dissolution of calcite and precipitation of Mg-bearing magnesite or Mg-rich carbonate have been identified, while during seawater injection (which contains sulfate) minerals such as anhydrite can also form (Madland et al. 2011; Minde et al. 2018). The Ca-Mg interactions appear to be substitution-like in the sense that as many Ca-ions dissolve as Mg^{2+}-ions precipitate (Korsnes et al. 2006; Madland et al. 2011). In long term tests with $MgCl_2$ that demonstrated strong rock compositional alterations, the porosity and permeability were not strongly affected (Nermoen et al. 2015). Studies have however indicated that non-carbonate minerals, especially reactive Si-bearing ones, can dissolve and further interact with Mg and form secondary Si-Mg-species, possibly talc, that drastically reduce the permeability (Madland et al. 2011; Andersen et al. 2018). The models have thus been able to link the change in injected and produced fluid composition to reaction kinetics of the key minerals. In recent years, more information has been made available regarding how the chemical alterations take place locally in the core. By dividing the flooded core into several slices after

the experiment, each slice could be analyzed for changes in composition, porosity, specific surface area, etc, which allows even more accurate quantification of the brine-rock interactions (Zimmermann et al. 2015; Andersen et al. 2018; Minde et al. 2018). At the current stage the models can replicate the observed temporal effluent profiles and spatial mineralogical alterations to great extent. There are also models that capture how changes in solid volume (calculated from produced and retained ions) and pore volume due to reactions and compaction affect porosity (Nermoen et al. 2015). Less emphasis has however been put towards incorporating how reaction kinetics and compaction are coupled in the models.

This work will attempt to link reactive flow with compaction during creep by interpretation of experimental data. A well-defined system with systematic changes in experimental conditions is considered. It is assumed that mainly reactive flow affects the compaction process (while the opposite relation is ignored) and suggest a link for how this occurs. Generally compaction should also affect flow and reactions, e.g. by restricting permeability, residence time, surface area or pressure solution (Hellmann et al. 2002). More comprehensive models considering compaction alone on bulk level can be found in Cristescu (1994) and Dahou et al. (1995). See also Barenblatt & Prostokishin (1993) for a modeling approach suggesting that material damage (crack propagation) diffuses spatially. A goal of the selected approach is that the model remains intuitive and that analytical solutions are obtained. This forms a basis for which stronger complexity can be implemented in future works.

The paper is structured as follows: Relevant chemistry and transient equations describing reactive flow; Analytical solutions for steady state ion and dissolution rate distributions at given injection conditions; Proposed mechanisms for chalk compaction in terms of pore volume reduction (driven by effective stress), solid volume alterations (chemistry) and chemical weakening (a coupling between the two); The steady state reactive flow solution is then combined with the compaction model to match and interpret experimental data from the literature.

Description of Experimental Setup

The system we attempt to model is chemical creep compaction of chalk core plugs. Experimentally, the core is loaded hydrostatically to reservoir-like effective stresses (defined by equal axial and radial stress and the pore pressure) and heated to the desired temperature. Injection of a specified brine (Ca-Mg-Na-Cl mixtures) is performed at fixed rate. When the core has been loaded to a stress state above yield (where the strain-stress relation becomes non-linear) the external stresses and pore pressure are set constant, while injection ensues. Compaction vs time at fixed stress (creep) is then studied together with the chemical response in effluent concentrations for periods of months. We refer to works such as Madland et al. (2011) for a more detailed description of the procedure.

Mathematical Modelling

The chemical compaction process is modelled as follows:

1) Relevant ions and minerals are selected. Analytical solutions are derived for steady state reactive flow. Dissolution rate and ion concentrations along the core are obtained as explicit functions of injected composition, reaction parameters and injection rate.
2) A model for creep compaction without chemical effects is suggested, accounting for variations in porosity and stress conditions. It allows modelling compaction tests where inert brines are flooded.
3) The compaction model is coupled to chemistry via the dissolution rate allowing modelling of chemical compaction tests.

The main assumptions considered are:

- The chemistry of the relevant system can be simplified to substitution-like processes.
- Compaction (changes in porosity and cross section) or other alterations of the system do not affect the interstitial velocity or the reaction parameters.
- Steady state between reaction and advection is established immediately after changing injected brine composition or injection rate. Dispersion is negligible compared to these effects.
- Compaction rate depends on porosity, chalk type and dissolution rate.

Reactive flow

Reactions and Transport Equations

We focus our study on injection of Ca-Mg-Na-Cl brines into pure chalk where the ions Ca and Mg are reactive due to mineral alternating processes and cation exchange. Experimental and modelling studies (Madland et al. 2011; Megawati 2011, 2015; Andersen et al. 2012, 2018; Minde et al. 2018) have shown that the main mineralogical interactions are dissolution of calcite $CaCO_3$ and precipitation of magnesite $MgCO_3$. The overall process appears to occur in a substitution-like manner, i.e. the same excess moles Ca are produced as moles Mg retained. The mineralogical and surface interactions, respectively, can be formulated as:

$$\mathrm{CaCO_3(s) + Mg^{2+}(aq) \leftrightarrow MgCO_3(s) + Ca^{2+}(aq)}, \tag{1}$$

$$\mathrm{CaX_2 + Mg^{2+}(aq) \leftrightarrow MgX_2 + Ca^{2+}(aq)}. \tag{2}$$

X^- denotes a free surface site. Na-Cl ions induce negligible impact. The following advection-dispersion-reaction partial differential equations describe the system (a similar form is found in Appelo and Postma (2004); Evje et al. (2009); Andersen et al. (2012)):

$$\partial_t(C_{ca} + \beta_{ca} CEC) = -\partial_x(v_w C_{ca}) + \partial_x(D\partial_x C_{ca}) + \dot{r}, \tag{3}$$

$$\partial_t\big(C_{mg} + \beta_{mg} CEC\big) = -\partial_x\big(v_w C_{mg}\big) + \partial_x\big(D\partial_x C_{mg}\big) - \dot{r}, \tag{4}$$

$$\partial_t(C_{nacl}) = -\partial_x(v_w C_{nacl}) + \partial_x(D\partial_x C_{nacl}), \tag{5}$$

$$\partial_t(\rho_c) = -\dot{r}, \tag{6}$$

$$\partial_t(\rho_m) = \dot{r}. \tag{7}$$

The left hand side represents storage terms where C_i, ρ_i and $\rho_i^s = \beta_i CEC$ denote brine, mineral and surface concentrations in mol per L initial pore volume. On the right hand side the advective terms represent bulk movement of brine with interstitial velocity v_w (the average pore velocity), dispersion terms with dispersion coefficient D account for Fick's law and the source term $\dot{r}$ (in mol per L pore volume per s) represents interactions due to calcite dissolution and magnesite precipitation. The source terms for the different species are of equal magnitude, but with sign according to the stoichiometry of (1)). β_i (i=*ca, mg*) are cation equivalent fractions and CEC is cation exchange capacity (mol per L pore volume). We use notation $C_{nacl} = \frac{1}{2}(C_{na} + C_{cl})$ as Na and Cl have identical tracer behavior. The reaction rate $\dot{r}$ is assumed to take the following form:

$$\dot{r} = k_1\big(C_{mg} - k_2 C_{ca}\big)^n, \tag{8}$$

where k_1 $\left[1/\left(\frac{\mathrm{mol}}{\mathrm{m^3}}\right)^{n-1}/\mathrm{s}\right]$ is a rate coefficient, k_2 $[-]$ is a reaction constant and n $[-]$ is the reaction order. At high C_{mg} and low C_{ca}, calcite dissolution and magnesite precipitation is triggered. The reaction (1) is in equilibrium when $\dot{r} = 0$ for any equilibrium composition $\big(C_{ca}^{eq}, C_{mg}^{eq}\big)$. Using this condition in (8) we see that:

$$k_2 = \frac{C_{mg}^{eq}}{C_{ca}^{eq}}. \tag{9}$$

k_2 is assumed temperature dependent, but constant for a given temperature (see **Appendix A)**). The surface exchange reaction (2) is instantaneous giving distributions of surface and brine species according to (Appelo & Postma 2004):

$$K = \frac{\beta_{mg} C_{ca}}{\beta_{ca} C_{mg}}. \tag{10}$$

We remark that the chemical reaction rates and equilibria in (8), (9) and (10) more generally should be functions of chemical activities (Langmuir 1997; Appelo & Postma 2004). However, by expressing equilibria and their constants in terms of the concentrations ratios (such as K and k_2), activity coefficients and complexation effects are implicitly accounted for.

Temperature

Reaction kinetics and equilibria are sensitive to temperature. The reaction rate coefficient k_1 is assumed to vary with (absolute) temperature T by an Arrhenius type relation (Langmuir 1997; Appelo & Postma 2004):

$$k_1(T) = k_1(T_{130}) \exp\left[\frac{E_a}{R}\left(\frac{1}{T_{130}} - \frac{1}{T}\right)\right]. \quad (11)$$

where $k_1(T_{130})$ is the rate coefficient at 130 °C which is the reference temperature, E_a is a representative activation energy of the reaction (1) and R is the universal gas constant. We refer to **Appendix A)** for the relation of the second reaction rate parameter $k_2(T)$. n was assumed constant.

Initial and boundary conditions

Initial conditions are specified for the system by three brine concentrations, two surface equivalent fractions and two mineral concentrations:

$$C_i(x, t = 0) = C_i^0, \qquad (i = ca, mg, nacl), \quad (12)$$

$$\beta_i(x, t = 0) = \beta_i^0, \qquad (i = ca, mg), \quad (13)$$

$$\rho_i(x, t = 0) = \rho_i^0, \qquad (i = c, m). \quad (14)$$

The initial brine must have zero reaction rate and be in equilibrium with the surface:

$$C_{mg}^0 = k_2 C_{ca}^0, \quad (15)$$

$$\beta_{mg}^0 C_{ca}^0 = \beta_{ca}^0 C_{mg}^0 K. \quad (16)$$

Note that if $C_i^0 = 0$ then both sides of (16) equal zero and the surface initial composition can be set freely (there are no ions in the brine to exchange with). The composition at the inlet boundary $x = 0$ is set constant during the time period $t_i < t < t_{i+1}$ as given by:

$$C_i(x = 0, t_i < t < t_{i+1}) = C_i^{inj}, \qquad (i = ca, mg, nacl). \quad (17)$$

Steady State

Steady state is defined by $\partial_t C_i = 0$ and $\partial_t \beta_i = 0$ at any location. A dynamic equilibrium is established between the advection, dispersion, surface and mineralogical processes. This state is described by explicit analytical solutions where dispersion is ignored ($D = 0$). Analytical solutions accounting for transient behavior and dispersive terms, although limited to $n = 1$, exist in integral form, see p. 61 in Logan (2013)). With the stated assumptions, the transport equations yield:

$$d_x(v_w C_{ca}) = \dot{r}, \quad (18)$$

$$d_x(v_w C_{mg}) = -\dot{r}, \quad (19)$$

$$d_x(v_w C_{nacl}) = 0, \quad (20)$$

$$\partial_t(\rho_c) = -\dot{r}, \quad (21)$$

$$\partial_t(\rho_m) = \dot{r}. \quad (22)$$

Although $\partial_t C_i = 0$ at steady state we may still have $\partial_t \rho_i \neq 0$ due to nonzero reaction rate $\dot{r}$. Due to the substitution-like behavior between Ca^{2+} and Mg^{2+}, the sum of their concentrations is preserved and identical to the injected value:

$$C_{ca}(x) + C_{mg}(x) = C_{ca}^{inj} + C_{mg}^{inj} \quad (23)$$

By using the definition of $\dot{r}$ in (8) together with (23) we can solve Eqs. (18) to (20) to obtain spatial profiles of ion concentrations $C_i(x)$ and reaction rate $\dot{r}(x)$. The following solutions, of exponential form, are obtained if reaction order $n = 1$ is used:

$$C_{ca}(x) = C_{ca}^{eq} - \left(C_{ca}^{eq} - C_{ca}^{inj}\right) \exp\left[-N_{Da,1}\frac{x}{L}\right], \quad (24)$$

$$C_{mg}(x) = C_{mg}^{eq} + \left(C_{mg}^{inj} - C_{mg}^{eq}\right) \exp\left[-N_{Da,1}\frac{x}{L}\right], \quad (25)$$

$$C_{nacl}(x) = C_{nacl}^{inj}, \quad (26)$$

$$\dot{r}(x) = k_1\left(C_{mg}^{inj} - k_2 C_{ca}^{inj}\right)\exp\left[-N_{Da,1}\frac{x}{L}\right], \quad (n = 1). \tag{27}$$

while the following solutions are obtained for reaction order $n \neq 1$:

$$C_{ca}(x) = C_{ca}^{eq} - \left(C_{ca}^{eq} - C_{ca}^{inj}\right)\left[1 + \left(\frac{C_{ca}^{eq} - C_{ca}^{inj}}{C_{mg}^{inj} - k_2 C_{ca}^{inj}}\right)^{n-1} N_{Da,n}\frac{x}{L}\right]^{\frac{1}{-n+1}}, \tag{28}$$

$$C_{mg}(x) = C_{mg}^{eq} + \left(C_{mg}^{inj} - C_{mg}^{eq}\right)\left[1 + \left(\frac{C_{mg}^{inj} - C_{mg}^{eq}}{C_{mg}^{inj} - k_2 C_{ca}^{inj}}\right)^{n-1} N_{Da,n}\frac{x}{L}\right]^{\frac{1}{-n+1}}, \tag{29}$$

$$C_{nacl}(x) = C_{nacl}^{inj}, \tag{30}$$

$$\dot{r}(x) = k_1\left(C_{mg}^{inj} - k_2 C_{ca}^{inj}\right)^n\left[1 + \frac{1}{(1+k_2)^{n-1}} N_{Da,n}\frac{x}{L}\right]^{\frac{n}{-n+1}}, \quad (n \neq 1). \tag{31}$$

Equilibrium concentrations C_{ca}^{eq}, C_{mg}^{eq} follow as function of the injected composition $C_{ca}^{inj}, C_{mg}^{inj}$ and k_2, see (32) and (33). We obtain a dimensionless Damköhler number $N_{Da,n}$, see (34) or (35), expressing the ratio of residence time (L/v_w) to a representative reaction time scale (see similar definitions and more detailed discussions of applications in Kee et al. 2005 and Fogler 2006). For large $N_{Da,n}$ the brine interacts strongly during its residence time.

$$C_{ca}^{eq}\left(C_{ca}^{inj}, C_{mg}^{inj}\right) = \frac{C_{ca}^{inj} + C_{mg}^{inj}}{1 + k_2}, \tag{32}$$

$$C_{mg}^{eq}\left(C_{ca}^{inj}, C_{mg}^{inj}\right) = \frac{k_2\left(C_{ca}^{inj} + C_{mg}^{inj}\right)}{1 + k_2}, \tag{33}$$

$$N_{Da,1} = (1 + k_2)\frac{k_1 L}{v_w}, \tag{34}$$

$$N_{Da,n} = (1 + k_2)^n \frac{k_1 L}{v_w}\left(C_{mg}^{inj} - k_2 C_{ca}^{inj}\right)^{n-1}(n - 1). \tag{35}$$

The reaction rate distribution is fixed with time, thus (21) and (22) can be integrated directly. The change in local mineral concentration is directly proportional to the time interval and the local reaction rate:

$$\rho_c(x,t) = \rho_c(x, t = t_i) - \dot{r}(x)[t - t_i], \tag{36}$$

$$\rho_m(x,t) = \rho_m(x, t = t_i) + \dot{r}(x)[t - t_i], \tag{37}$$

where $\dot{r}(x)$ is given by (27) or (31). Considering the expressions for $\dot{r}(x)$, the highest reaction rate is found at the inlet and is simply evaluated by (8) at the injected composition. The reaction rate gradually approaches zero with distance, and the brine concentrations approach C_i^{eq}.

Compaction Modelling

Terminology

Consider a core with length L, diameter d_c, solid volume V_s, pore volume V_p and bulk volume $V_b = V_p + V_s$ at a given time. Original values of these parameters are denoted by 0, see **Figure 1 left**. The core is compacting while being flooded with brine. Local compaction is studied in terms of thin slice elements along the axial direction, see **Figure 1 right**. Slice element j (counting from 1 at the inlet) has bulk volume $\delta V_j = \frac{\pi}{4} d_{cj}^2 \delta L_j$ where d_{cj} is the slice diameter and δL_j the slice length. Note that $\sum_j \delta L_j = L$, i.e. the length of the slices adds to the total length of the core. The slice volume δV_j consists of a solid part V_{sj}

and a porous part V_{pj} such that:

$$\delta V_j = \delta V_{sj} + \delta V_{pj}. \quad (38)$$

The index j is skipped in the following.

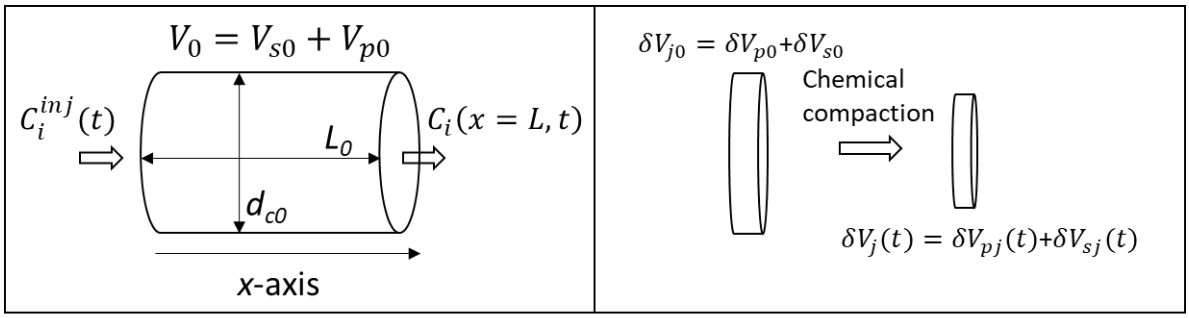

Figure 1 System geometry. Left: A core with initial dimensions L_0, d_{c0} is flooded with brine composition C_i^{inj} and corresponding effluent concentration $C_i(x = L, t)$ leaves the core. The initial bulk volume consists of a solid part V_{s0} and porous part V_{p0}. Right: The core is studied locally by individual slice segments j with original volumes δV_{j0} that change with time due to chemical compaction into $\delta V_j(t)$.

During the flooding-compaction tests the core deforms locally (in each slice) due to alterations in one or both of these fractions.

$$d\delta V = \left(\frac{\partial \delta V}{\partial \delta V_p}\right)_{\delta V_s} (d\delta V_p)_{\delta V_s} + \left(\frac{\partial \delta V}{\partial \delta V_s}\right)_{\delta V_p} (d\delta V_s)_{\delta V_p} = (d\delta V_p)_{\delta V_s} + (d\delta V_s)_{\delta V_p}. \quad (39)$$

The lower index in the partial derivatives and differentials indicates the variable held constant. We consider two main mechanisms:

- *Stress accommodation*: The pore volume δV_p (via porosity ϕ) adjusts to reduce the stress carried by the core. The minerals are assumed to have constant density and the solid volume δV_s is therefore not reduced by compaction.
- *Chemical alteration and weakening*: Mineral dissolution and precipitation changes the mineralogical composition and the non-porous volume δV_s. Alterations in solid volume can be quantified from effluent data and mineral densities. Changes in compaction parameters compared to inert brine systems are related to chemical weakening effects. A correlation to dissolution rate is proposed and quantified.

During a time interval both volumes in (39) will change. We demonstrate how each of them are calculated over a time interval from t_i to $t_i + \Delta t$ while keeping the other constant. The change in bulk volume with time follows from (39) as:

$$\delta V(t_i + \Delta t) - \delta V(t_i) = \left(\delta V_p(t_i + \Delta t) - \delta V_p(t_i)\right)_{\delta V_s} + \left(\delta V_s(t_i + \Delta t) - \delta V_s(t_i)\right)_{\delta V_p}. \quad (40)$$

Stress Accommodation

Stress accommodation by pore volume reduction is represented by the first term on the RHS of (39). We here propose how pore volume and porosity in a slice change while keeping solid volume fixed.

The driving mechanism for rock deformation is effective stress σ' (Jaeger & Cook 1976; Fjær et al. 1992), defined as stress σ minus pore pressure p_f multiplied by Biot factor β:

$$\sigma' = \sigma - \beta p_f, \quad (41)$$

which is isotropic due to the hydrostatic conditions. During elastic compaction (before yield) a well-defined equilibrium state exists for each effective stress. As the stress state is increased sufficiently beyond yield (the stress where linear deformation ends), deformation does not occur incrementally, but even for a fixed stress continues indefinitely (Andersen et al. 1992) due to the continuous breaking of mineral bonds on microscale. This condition is termed creep deformation and is our focus.

The confining pressure P_{con} exerts a force on the core that is counteracted by a force from the

matrix $F_m f(\phi)$ where $f(\phi)$ is the load-bearing non-porous surface fraction (which may less than $1-\phi$) and the force supported by the fluid in the pores $P_f\beta$ where β is the Biot coefficient. This balance yields:

$$P_{con} = F_m f(\phi) + P_f\beta, \qquad \rightarrow \qquad F_m = \frac{P_{con} - P_f\beta}{f(\phi)} = \frac{\sigma'}{f(\phi)}. \tag{42}$$

Note that F_m represents stress in terms of force per loadbearing area of matrix. We propose that this quantity is directly related to the rock's deformation. Loadbearing area is generally unknown or varying with time or even spatially in the core. Thus, the macroscopic quantity σ' is more often applied to describe the stress state. To explain experimental observations, we must however allow changes in porosity to affect the compaction rate making F_m a more relevant parameter. The following rate law is proposed:

$$\frac{d\phi}{dt} = -k_c(\dot{r})F_m(\phi), \tag{43}$$

$$F_m = \left[\left(\phi_y + \Delta\phi\right) - \phi\right]^m. \tag{44}$$

k_c [1/Pa/s] is a compaction (rate) coefficient and m [−] is an exponent. ϕ_y is the porosity at the start of creep compaction (close to yield). Both k_c and m describe the rock's response in compaction rate to changes in porosity and are considered chalk dependent. The above relation has the following features:

- The rate of porosity change with time is proportional to F_m (and σ'). A higher confining pressure or lower pore pressure will enhance the compaction rate.
- F_m is reduced when porosity is reduced, hence the compaction rate decreases with time, in line with observations.
- At yield the core has porosity ϕ_y. Due to the initiation of creep a low area fraction $F_m(\Delta\phi)$ is loadbearing. This allows a high compaction rate at onset of creep (infinite if $\Delta\phi = 0$).

By definition of creep σ' is constant with time and uniform. As indicated we let k_c vary locally depending on dissolution rate (see ***Chemical Weakening***), but consider time intervals $t_i < t < t_{i+1}$ where it does not change with *time*. Integrating (43) with (44) then yields the following porosity evolution with time:

$$\phi(t) = \left(\phi_y + \Delta\phi\right) - \left[\left(\phi_y + \Delta\phi\right) - \phi(t_i)\right]\left[1 + \frac{(m+1)k_c\sigma'(t-t_i)}{\left[\left(\phi_y + \Delta\phi\right) - \phi(t_i)\right]^{m+1}}\right]^{\frac{1}{m+1}}. \tag{45}$$

Nermoen et al. (2016) also suggested a compaction law for creep as function of porosity, but assumed compaction would stop at a critical porosity. The rate law proposed here also bears similarity to that proposed by Andersen et al. (1992) giving logarithmic compaction with time also allowing a high or infinite rate at start of creep and not predicting compaction to stop. Using the definition of porosity $\left(\phi = \frac{\delta V_p}{\delta V_p + \delta V_s}\right)$, the differential change in pore volume, for fixed solid volume, is:

$$\left(d\delta V_p\right)_{\delta V_s} = \delta V_s d\left(\frac{\phi}{1-\phi}\right). \tag{46}$$

which integrates to:

$$\delta V_p(t) = \delta V_p(t_i) + \delta V_s(t_i)\left(\frac{\phi(t)}{1-\phi(t)} - \frac{\phi(t_i)}{1-\phi(t_i)}\right), \qquad (t_i < t < t_{i+1}). \tag{47}$$

where $\phi(t)$ is obtained from (45).

Chemical Alteration

Mineral concentrations ρ_i are relative to the initial pore volume such that the solid volume δV_s of minerals in a slice is given by:

$$\delta V_s = \sum_{i:c,m}\left[\frac{\rho_i M_{wi}}{\omega_i}\right]\delta V_{p0} = \left[\frac{\rho_c M_{wc}}{\omega_c} + \frac{\rho_m M_{wm}}{\omega_m}\right]\delta V_{p0}. \tag{48}$$

M_{wi} [kg/mol] is mineral molar weight and ω_i [kg/m^3] is mineral density. We also make use of the substitution-relation between calcite and magnesite from (1):

$$\rho_c + \rho_m = \rho_c^0 + \rho_m^0. \tag{49}$$

The solid volume can then be expressed as $\delta V_s(\rho_m)$:

$$\delta V_s = \left[\frac{(\rho_c^0 + \rho_m^0 - \rho_m)M_{wc}}{\omega_c} + \frac{\rho_m M_{wm}}{\omega_m}\right]\delta V_{p0}. \tag{50}$$

The initial concentrations must be related to the initial porosity such that $\frac{\delta V_{s0}}{\delta V_{p0}} = \frac{\delta V_s(\rho_i^0)}{\delta V_{p0}} = \frac{1-\phi_0}{\phi_0}$, giving:

$$\frac{\rho_c^0 M_{wc}}{\omega_c} + \frac{\rho_m^0 M_{wm}}{\omega_m} = \frac{1-\phi_0}{\phi_0}. \tag{51}$$

Considering originally pure chalk, we have $\rho_m^0 = 0$ and the above formulas simplify to (the first relation also found in Andersen et al. 2012):

$$\rho_c^0 = \frac{\omega_c}{M_{wc}}\frac{1-\phi_0}{\phi_0}, \tag{52}$$

$$\delta V_s(\rho_m) = \left[\frac{(\rho_c^0 - \rho_m)M_{wc}}{\omega_c} + \frac{\rho_m M_{wm}}{\omega_m}\right]\delta V_{p0}. \tag{53}$$

The differential in solid volume is:

$$(d\delta V_s)_{\delta V_p} = \left[\frac{M_{wm}}{\omega_m} - \frac{M_{wc}}{\omega_c}\right]\delta V_{p0} d\rho_m = \left[\frac{M_{wm}}{\omega_m} - \frac{M_{wc}}{\omega_c}\right]\delta V_{p0}\dot{r}dt. \tag{54}$$

where the relation (37) was used in the last equality. By integration we get:

$$\delta V_s(t) = \delta V_s(t_i) + \left[\frac{M_{wm}}{\omega_m} - \frac{M_{wc}}{\omega_c}\right]\delta V_{p0}\dot{r}(t - t_i). \tag{55}$$

Note that the change in solid volume is directly proportional to the reaction rate. From literature, the value of the factor $\frac{M_{wm}}{\omega_m} - \frac{M_{wc}}{\omega_c}$ is -8.80 mL/mol. Its negative value indicates that the solid volume is reduced when 1 mol calcite is replaced by 1 mol magnesite. The porous volume is held fixed before and after the change in solid volume, but their proportion changes giving a new porosity:

$$\delta V_p = \frac{\delta V_s(t_i)\phi(t_i)}{1-\phi(t_i)} = \frac{\delta V_s(t_{i+1})\phi(t_{i+1})}{1-\phi(t_{i+1})}, \tag{56}$$

which is solved to give:

$$\phi(t_{i+1}) = \frac{\delta V_p}{\delta V_s(t_{i+1}) + \delta V_p}. \tag{57}$$

Chemical Weakening

Experimental measurements (Korsnes et al. 2006; Madland et al. 2011) have indicated that compaction increases with dissolution of calcite. Such relations are incorporated by letting the compaction coefficient k_c in (43) vary with the dissolution rate of calcite $\dot{r}$ using an exponential relation:

$$k_c(\dot{r}) = k_{c0} + (k_c^{max} - k_{c0})\frac{\exp(\dot{r}/\dot{r}_{ref}) - 1}{\exp(\dot{r}_{max}/\dot{r}_{ref}) - 1}, \tag{58}$$

$$k_c(\dot{r}_{max}) = k_c^{max}, \;\; k_c(0) = k_{c0}. \tag{59}$$

k_{c0} [1/Pa/s] is the compaction coefficient at zero dissolution rate, k_c^{max}[1/Pa/s] is the compaction coefficient associated with the highest dissolution rate $\dot{r}_{max}$ considered under the presented experimental conditions. The latter is found by evaluating the reaction rate with the most reactive composition (the brine with highest Mg concentration $C_{mg} = 0.219$ M and lowest Ca concentration $C_{ca} = 0$ M) and (highest) temperature 130 °C, i.e.:

$$\dot{r}_{max} = k_1(T_{130})\left(C_{mg}^{max}\right)^n \tag{60}$$

If $k_c^{max} = k_{c0}$, chemistry does not affect the compaction coefficient (solid volume changes can still

occur). Note that $\dot{r}_{max}$ is independent of k_2. $\dot{r}_{ref}$ is an arbitrarily valued tuning parameter (positive or negative). An illustration of how it impacts (58) is given in **Figure 2**.

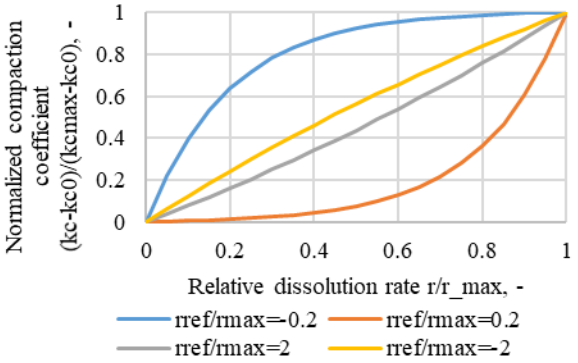

Figure 2 Proposed correlation between min and max compaction rate vs dissolution rate. For $\left|\frac{r_{ref}}{r_{max}}\right| > 2$ the relation is close to linear. For $\frac{r_{ref}}{r_{max}} < 0$ high compaction rate is obtained for low dissolution rates, while for $\frac{r_{ref}}{r_{max}} > 0$ high dissolution rates are required to increase the compaction rate.

Overall Compaction

From the above calculations we obtain the evolution of solid, porous and bulk volume and porosity in each slice j as function of time. As we consider isotropic stresses we assume the deformation in each slice is isotropic:

$$\frac{d_{cj}(t)}{d_{c0}} = \frac{\delta L_j(t)}{\delta L_0}. \tag{61}$$

which implies:

$$\delta L_j = \delta L_0 \left(\frac{\delta V_j}{\delta V_0}\right)^{\frac{1}{3}}, \tag{62}$$

$$d_{cj} = d_{c0} \left(\frac{\delta V_j}{\delta V_0}\right)^{\frac{1}{3}}. \tag{63}$$

Axial strain ϵ_{aj} and radial strain ϵ_{rj} (along the core) are defined by their reduction from initial value, divided by their initial value:

$$\epsilon_{aj} = \frac{\delta L_0 - \delta L_j}{\delta L_0}, \tag{64}$$

$$\epsilon_{rj} = \frac{d_{c0} - d_{cj}}{d_{c0}}. \tag{65}$$

The length L and axial strain of the entire core $\bar{\epsilon}_a$ as function of time is given by:

$$L(t) = \sum_j \delta L_j, \tag{66}$$

$$\bar{\epsilon}_a = \frac{L_0 - L(t)}{L_0}. \tag{67}$$

Finally, the volume V and volumetric strain of the entire core $\bar{\epsilon}_v$ is found by:

$$V(t) = \sum_j V_j, \tag{68}$$

$$\bar{\epsilon}_v = \frac{V_0 - V(t)}{V_0}. \tag{69}$$

For uniform deformation at small strains it can be shown by combination of the above equations (61) to (68) and Taylor expansion that $\epsilon_a = \epsilon_r = \frac{1}{3}\epsilon_v$ as also pointed out by Fjær et al. (1992). Nermoen et al.

(2015) derived a relation between changes in solid volume and pore volume and effluent measurements and strain evolution to estimate average porosity evolution with time. No physical model was assumed, hence only average properties were linked and the model was not predictive in terms of future compaction or sensitivity to experimental parameters.

Solution procedure

The system was described using $N_j = 60$ cells along the flow direction and $N_t = 500$ or 5000 time splitting steps Δt (summing to the total time) if tests of less or more than 100 d were considered, respectively. The core was assigned initial dimensions L_0, d_{c0}, ϕ_0 yielding initial mineral concentration ρ_{c0} from (52) and initial slice volumes $\delta V_j^0, \delta V_{pj}^0, \delta V_{sj}^0$. At a given time step, knowing the injected brine composition C_i^{inj} and injection rate; the steady state distributions of brine concentrations and dissolution rate were calculated using Eqs. (24) to (32). Knowing the porosity distribution and $\dot{r}$, the core slice pore volumes δV_{pj} and porosities ϕ_j were updated from t_i to $t_i + \Delta t$ while holding the slice solid volume δV_{sj} constant, see (45) and (47). Following, the slice pore volume δV_{pj} was held constant and the slice solid volume δV_{sj} and mineral concentrations were also changed from t_i to $t_i + \Delta t$ due to mineral reactions by (55) and porosities were again updated by (57), finalizing one splitting step. See further details in **Appendix B)**.

Results and Discussion

First we present an overview of literature experimental data, their test conditions and the parameters involved in the simulations. A comparison is made between the full transient solution for reactive flow Eqs. (3) to (7) and its steady state solution (24) to (27) or (28) to (31). Without loss of generality, but for a more transparent analysis, the examples will interpret chemical compaction data only by applying the *steady state* reactive flow solution which, through the dissolution rate profile, affects the compaction rate.

Parameterization and Input

Experimental data from two chalk types, originating from Liege (Belgium) and Aalborg (Denmark), were considered separately as they displayed distinct chemo-mechanical behavior. Similar experimental conditions with systematic variations in injected brine composition and temperature were considered. Core labels, their properties and their sources are shown in **Table 1**. Unless otherwise stated the injection rate was 1 PV/d. The brine compositions, in terms of the variables of the model, are listed in **Table 2**. The stated dimensions, test conditions and porosities of the cores were within a narrow range as summarized in **Table 3** and representative values were used as simulation input for each chalk type as indicated.

Table 1 Core test parameters and initial dimensions as reported in the literature. The pore pressure was 0.7 MPa in all tests. The injection rate was 1 PV/d in all tests except L18. N/A: Not directly reported in source, typical permeability values for Liege are ~2 mD. The core labels are the same as in their source references.

Core label	Chalk Type	Injection brine	Reference	Tempe-rature (°C)	Duration (d)	ϕ_0 (%)	Perme-ability (mD)	d_0 (mm)	L_0 (mm)	P_{con} (MPa)
RL11	Liege	0.657 M NaCl	Madland et al. (2011)	130	13	41.2	N/A	37	70	10.5
RL14					12.6	41.1	N/A	37	70	10.5
RL2		0.219 M $MgCl_2$			13.7	41.1	N/A	37	70	10.5
RL16		0.109 M $MgCl_2$			19.8	41.2	N/A	37	70	10.5
RL5					7.8	41.4	N/A	37	70	10.5
LI1		0.219 M $MgCl_2$	Andersen et al. (2018)		65	43.3	1.92	37.1	68.9	10.5
LI2		0.657 M NaCl			90	43.3	1.75	38.2	72.7	9.5
LEM3		0.657 M NaCl, 0.219 M $MgCl_2$, 0.219 M MgCl2 + 0.13 CaCl2	Megawati et al. (2011)		~260	43	2.75	38	70	11.6
L18		0.219 M MgCl2	Nermoen et al. (2015)		1072	41.3	1.1	38	70	11.1
(A) LT		0.219 M $MgCl_2$	Zimmermann		516	40.5	N/A	38	70	12.6

			et al. (2015)							
ÅR1	Aalborg	0.219 M $MgCl_2$	Megawati et al. (2015)	130	~290	46.2	3-5	38	70	12
ÅR9					~290	46.5	3-5	38	70	12
ÅR2		0.657 M NaCl			~265	46.2	3-5	38	70	12
ÅR4					~265	46.7	3-5	38	70	12
Mg25		0.219 M $MgCl_2$	Minde et al. (2018)	25	61	47.9	5.24	37	71.8	10
Mg60				60	62	46.8	3.46	37	72.6	10
Mg92				92	60	47.1	2.58	38.1	69.2	11
Mg110				110	66	47.4	2.93	37.1	69.4	8
Mg130				130	61	47.2	1.52	38.1	70.4	11
LMg130				130	115	47.5	1.34	38.1	75	11
Na130		0.657 M NaCl		130	60	46.9	2.35	38.2	70.4	12
LNa130				130	118	47.5	1.79	37	70.4	12

Table 2 Injected or initial brine compositions C_i^{inj}, C_i^0 used in the examples. Note that M denotes mol/L, while DW denotes distilled water.

Brine	DW	0.657 M NaCl	0.109 M $MgCl_2$	0.219 M $MgCl_2$	0.219 M $MgCl_2$ + 0.13 M $CaCl_2$
C_{ca}	0	0	0	0	0.13
C_{mg}	0	0	0.109	0.219	0.219
C_{nacl}	0	0.657	0.109	0.219	0.349

Table 3 Experimentally measured parameter range (from Table 1) and representative values used for simulation input.

Chalk type		ϕ_0 (%)	P_{con} (MPa)	P_f (MPa)	d_{c0} (mm)	L_0 (mm)
Liege	Exp. range	40.5-43.3	9.5-12.6	0.7	37-38.2	68.9-72.7
	Sim. input	43	11	0.7	38	70
Aalborg	Exp. range	46.2-47.9	8-12	0.7	37-38.2	69.2-75
	Sim. input	47	12	0.7	38	70

First, reaction kinetics were determined. k_2 was estimated from geochemical equilibrium calculations. It was verified to have a unique value at a fixed temperature, but to be temperature dependent, see details in **Appendix A)**. Particularly, $k_2(130\ ^\circ\mathrm{C}) = 0.39$ and increasing with lower temperature. The reaction order was set to $n = 2$ based on Saldi et al. (2009) who measured magnesite precipitation rates at 100 °C. The remaining parameter k_1 was obtained by matching effluent and mineralogical profiles after flooding. If no match was found, the estimates of k_2 and n were reevaluated. The response in effluent data to compositional variations also indicate the quality of the reaction kinetic parameters. The temperature dependence of k_1 according to (11) was used to match experimental effluent trends with temperature. Changes in composition and temperature induce different magnitude of dissolution rates along the core which allows calibration of the compaction parameters.

Stress accommodation parameters k_{c0}, m in (44) and (58) were estimated from compaction tests with inert brines being flooded. The parameter $\Delta\phi$ was set 0 for both chalks. Then, knowing the dissolution rate distributions under different test conditions, the parameters $\dot{r}_{ref}$ and k_c^{max} were obtained to generate the correct trends in compaction in relation to reactiveness (induced via reactive brines or high temperature).

All the matched parameters are summarized in **Table 4**. For a given chalk type, the same parameters were used in all simulations showed.

Table 4 Model input parameters for reaction-compaction behavior based on matching Liege and Aalborg chalk experimental data. The activation energy was obtained for Aalborg only. The Biot coefficient was assumed to be 1.

Chalk dependent parameters	$k_1(T_{130})$ $\left(1/\left(\frac{\mathrm{mol}}{\mathrm{m}^3}\right)^{n-1}/\mathrm{s}\right)$	n (-)	m (-)	k_{c0} (1/Pa/s)	k_c^{max} (1/Pa/s)	$k_2(T_{130})$ $(-)$	E_a (kJ/mol)	$\dot{r}_{ref}$ $(\mathrm{mol/m^3/s})$	$\dot{r}_{max}$ $(\mathrm{mol/m^3/s})$	$\frac{\dot{r}_{ref}}{\dot{r}_{max}}$ $(-)$
Liege	$1.70 \cdot 10^{-8}$	2	2	$2.75 \cdot 10^{-19}$	$4 \cdot 10^{-18}$	4.5	N/A	$-1 \cdot 10^{-4}$	$7.91 \cdot 10^{-4}$	-0.13
Aalborg	$7.25 \cdot 10^{-9}$	2	1	$8.0 \cdot 10^{-18}$	$6.5 \cdot 10^{-17}$	0.39	30	$-5 \cdot 10^{-5}$	$3.47 \cdot 10^{-4}$	-0.14

Comparison of General and Steady State Models

A common feature of high temperature $MgCl_2$ injection tests is that Mg is retained and Ca is produced in the effluent. This is accounted for in the model by magnesite precipitation and calcite dissolution. Before this can take place throughout the core, the initial brine must be displaced, and a transition is seen where surface chemistry and mixing takes place. Eventually steady state is obtained. Dispersion can be of importance and affect the ionic distributions before and after steady state. Using the reaction kinetic parameters for Liege, see **Table 4**, the full reactive flow model (3) to (7) was compared with the steady state solution Eqs. (24) to (37) to model core test RL2 from Madland et al. (2011) where 0.219 M $MgCl_2$ was injected at 1 PV/d.

The simulated and experimental effluent concentrations are shown in **Figure 3** left. The early transient period with a Ca peak and Mg delay was captured using ion exchange, see (2). Steady state is achieved after ~6 to 10 PVs. In **Figure 3** right the dissolution rate profiles along the core are displayed. After 1 and 2 PV the profiles differ greatly from the steady state solutions. After 4 PVs the shape and magnitude are similar and after 10 PVs they are virtually identical. For the experimental data considered, 10s to 100s of PVs were injected. It is therefore reasonable to assume the transition period produces a negligible difference on the overall chemical alteration and compaction.

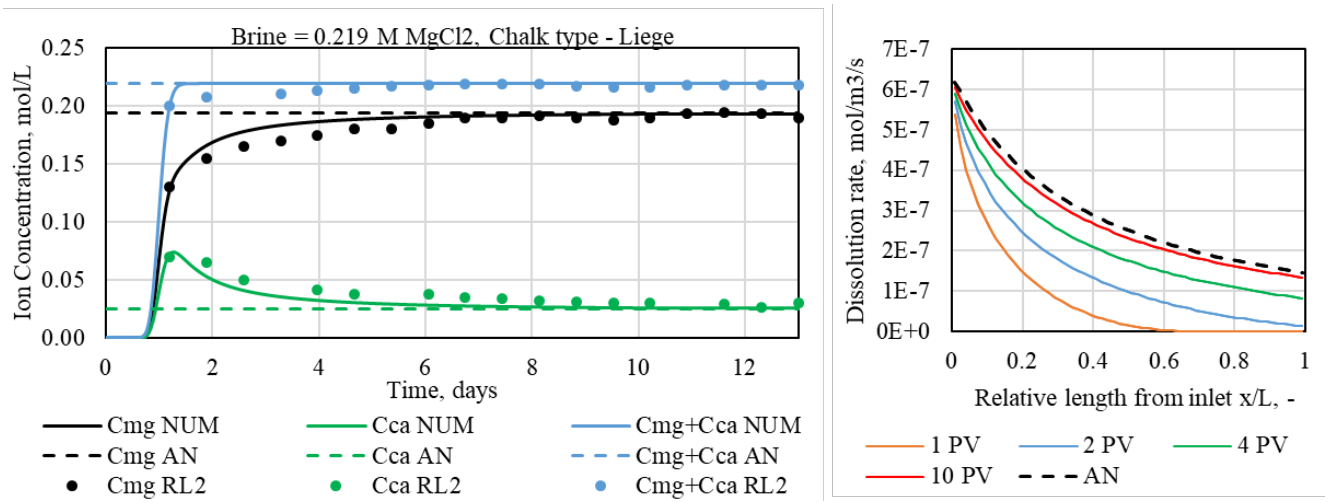

Figure 3 Left: Simulated and experimental effluent concentrations $C_{ca}(x = L, t), C_{mg}(x = L, t)$ and their sum based on test RL2 where 0.219 M $MgCl_2$ was flooded through Liege chalk at 1 PV/d. Both the full transient model (NUM) and analytical (AN) steady state models are compared. Right: Simulated spatial profiles of dissolution rate (right) after different amount injected PVs are shown for the numerical transient model and compared with the steady state analytical model.

Aalborg Chalk

Core tests ÅR1, Mg130 and LMg130 with injection of 0.219 M MgCl2 at 130 °C were matched in terms of steady state effluent measurements of C_{ca} and C_{mg} (**Figure 4** left) simultaneously with mineralogical alteration profiles along the core Mg130 after flooding (**Figure 4** right) by selecting a proper value for k_1. A good match of both was obtained with this one parameter supporting the selection of k_2 and n. The relatively uniform distribution of Mg mineral was captured with 1.4 times higher concentration at the inlet compared to the outlet.

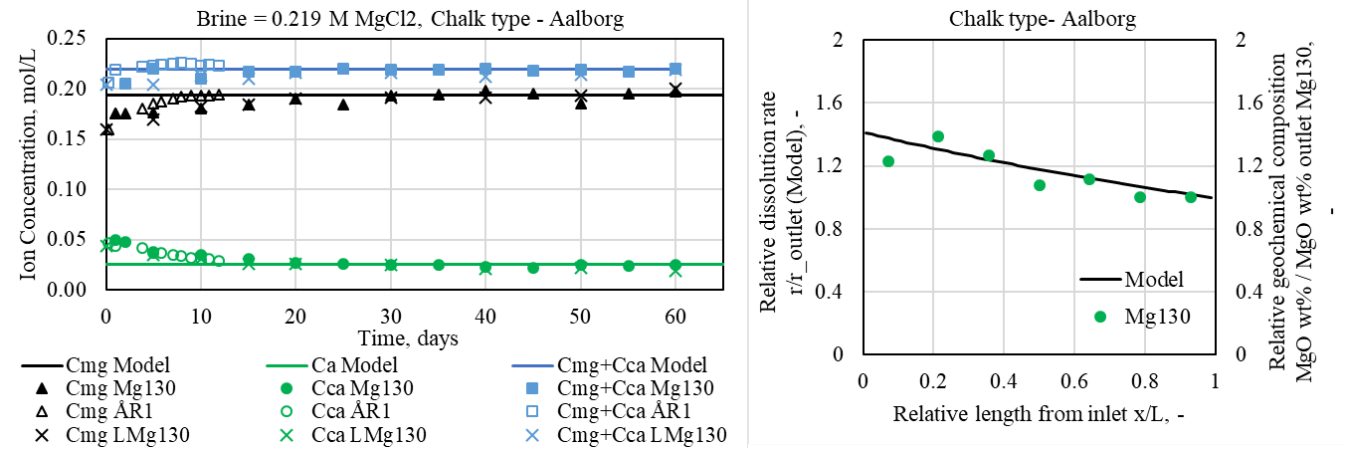

Figure 4 Left: Simulated (analytical model) and experimental effluent concentrations $C_{ca}(x = L, t), C_{mg}(x = L, t)$ and their sum based on tests ÅR1, Mg130 and LMg130 where 0.219 $MgCl_2$ brine was flooded through Aalborg chalk at 1 PV/d. Right: Comparison of reaction rate $\dot{r}$ (analytical model) along the core at steady state and observed mineralogical alteration in terms of MgO wt% in slices of the core AA5 cut after flooding 0.219 M $MgCl_2$. The values are scaled by the value at the outlet for direct comparison.

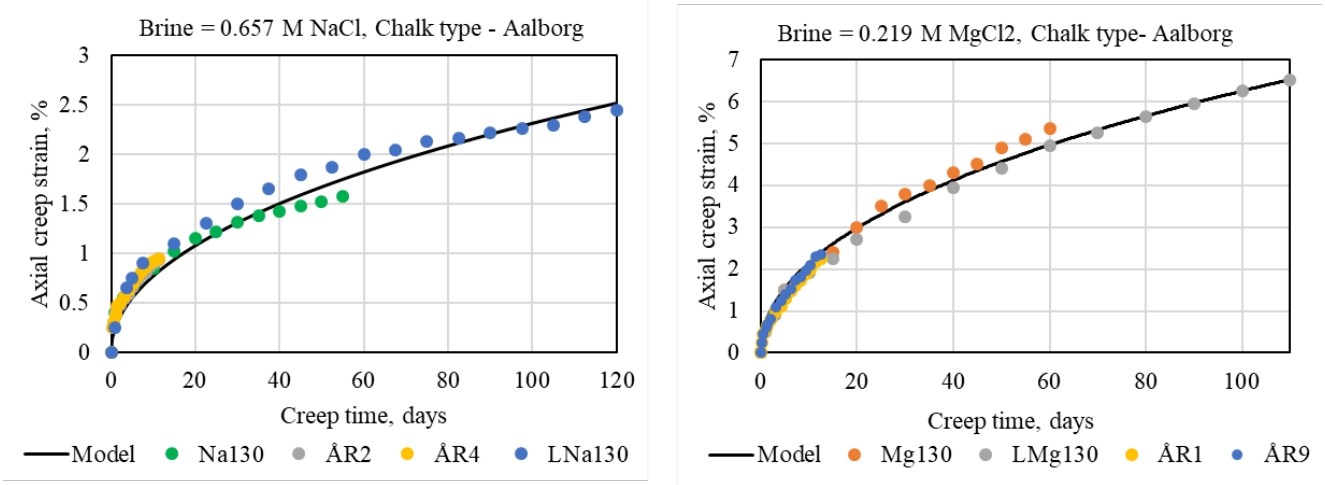

Figure 5 Comparison of simulated (analytical model) and experimental creep compaction at 130 °C in Aalborg chalk. Left: Tests where 0.657 M NaCl (inert brine) is injected at 1 PV/d. Right: Tests where 0.219 M MgCl2 is injected at 1 PV/d.

Creep compaction in NaCl flooded cores was matched in terms of axial creep strain, see **Figure 5** left. For these tests the dissolution rate is negligible and only the stress accommodation mechanism is relevant; no chemical weakening or solid volume changes were expected. Hence the parameters k_{c0} and m were estimated. Compaction during injection of 0.219 M $MgCl_2$ was also matched, see **Figure 5** right, by estimating k_c^{max} and $\dot{r}_{ref}$. Since m also affects the time trend of these tests both sets of data were tuned to give an overall match. Note that these two sets of data do not provide enough data to say how compaction rate changes with dissolution rate, i.e. more data were needed to get a more unique match of k_c^{max} and $\dot{r}_{ref}$.

Such data were provided by interpreting tests with injection of 0.219 M $MgCl_2$ at different temperatures, from ambient to 130 °C. The effluent data were matched by finding an appropriate E_a to reduce the reaction rate coefficient k_1 with temperature. The match is seen in **Figure 6** left for Ca and Mg concentrations. With this new information, multiple test conditions with different dissolution rate distributions along the core were obtained with corresponding compaction rates, see **Figure 6** right. By recalibrating k_c^{max} and $\dot{r}_{ref}$ the sensitivity in compaction between the inert and most reactive (130 °C) states was calibrated. Notably, there is little Ca production with $MgCl_2$ brine at ambient temperature, but a significant increase in compaction compared to NaCl. On the other hand; there is considerably lower Ca production at 110 °C compared to at 130 °C, but the compaction trends are overlapping. This suggests a strong sensitivity of compaction rate to dissolution rate at low dissolution rates, but less sensitivity at high

dissolution rates. It is noted that observed compaction at 60 °C and 25 °C closely overlapped and that compaction at 92 °C was lower than for these two tests. The 60 °C and 92 °C data hence did not follow smooth trends that could easily be captured.

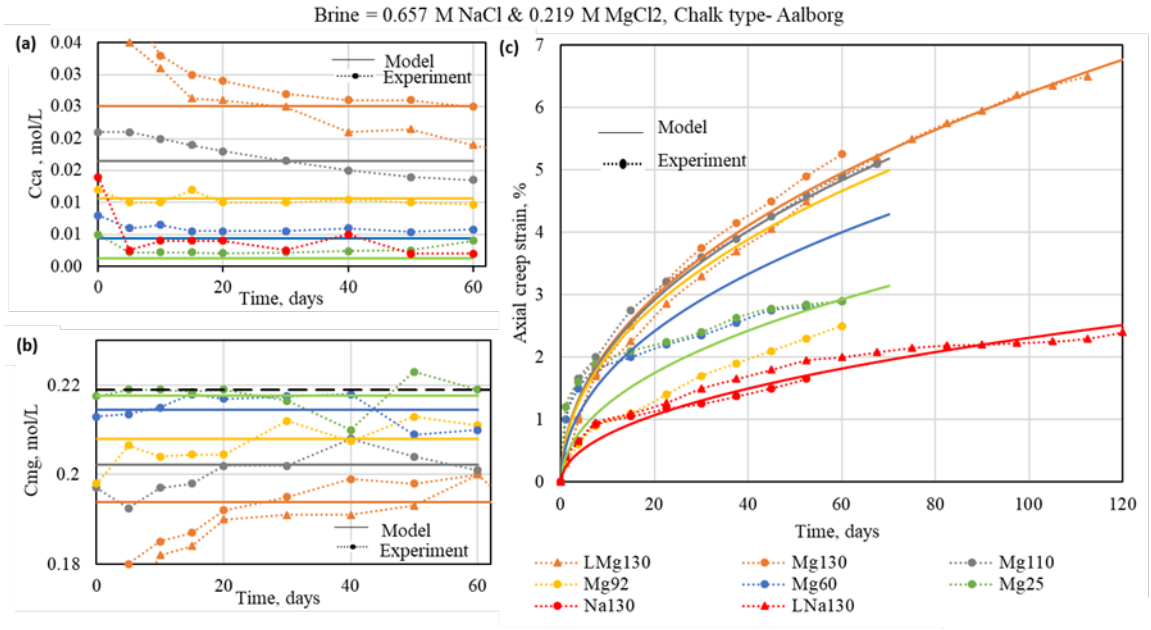

Figure 6 Left: Simulated (analytical model) and experimental Ca (top) and Mg (bottom) effluent concentrations for Aalborg tests where 0.219 M $MgCl_2$ was injected at 1 PV/d at different temperatures (indicated in core label by ℃) or 0.657 M NaCl at 130 °C. Right: Corresponding creep compaction profiles.

Liege Chalk

When interpreting the reaction chemistry for Liege several observations indicated that more than assigning a value to k_1 was required to explain the measurements. Four types of observations were used to match the reaction kinetics: Effluent data from tests with injection at 1 PV/d of 0.219 M $MgCl_2$ (**Figure 7a**), tests with 0.109 M $MgCl_2$ (**Figure 7b**), and a test with 0.219 M $MgCl_2$ mixed with 0.13 M $CaCl_2$ to minimize calcite dissolution in presence of Mg rich brine (0.219 M $MgCl_2$ without Ca had been injected prior and latter to that brine). The latter test, indeed demonstrated stable Ca and Mg effluent concentrations identical to the injected values (**Figure 7c**). Finally, mineralogical alteration profiles obtained after flooding from two cores where 0.219 M $MgCl_2$ had been injected at 1 PV/d for 516 and 65 d (**Figure 7d**). The two cores displayed similar distribution of Mg minerals after flooding mainly in the two last thirds from the inlet. In the third of the core near inlet the long term flooded core displayed highest Mg mineral presence near the inlet (~11 times more at the inlet peak than the outlet), while the other core had less Mg near the inlet than centrally (~3 times more at the central peak than at the outlet).

Assigning a value to k_1 while using the expected $n = 2$ and $k_2 = 0.39$ would be able to match the low and high injected concentration effluent measurements reasonably, but would predict significant dissolution with Ca spiked brine and a very flat mineral concentration profile, more in correspondence with Aalborg. Applying a higher reaction order n and selecting k_1 would allow matching 0.219 M $MgCl_2$ effluent measurements and the mineralogical profiles, but only with unreasonably high values of $n \approx 15$. Also, the response in composition was greatly mispredicted giving negligible interaction as soon as the composition was made slightly less reactive.

The data were matched by allowing the brine to reach an equilibrium at a higher Mg to Ca ratio (higher k_2) than suggested by geochemical calculations, which in principle means stable oversaturation. Stable oversaturated solutions have been reported in the literature (Land 1998). Applying a value of $k_2 = 4.5$ together with keeping $n = 2$ and selecting k_1 gave the right magnitude of effluent concentrations and mineralogical profiles. We note that for the Ca spiked brine the injected composition was inert and produced the ratio $\frac{C_{mg}}{C_{ca}} = 1.6 > 0.39$ (the predicted value from Phreeqc). This indicates that the solution

was stable while oversaturated, supporting our hypothesis. For $0.39 < \frac{c_{mg}}{c_{ca}} < 4.5$ the dissolution rate was thus set to 0 for Liege chalk. The fact that Aalborg chalk could be interpreted with the theoretical values (no stable oversaturation) could be related to the presence of reactive impurities such as Opal-CT (Andersen et al. 2018; Minde et al. 2018) enabling the reactions to proceed towards equilibrium.

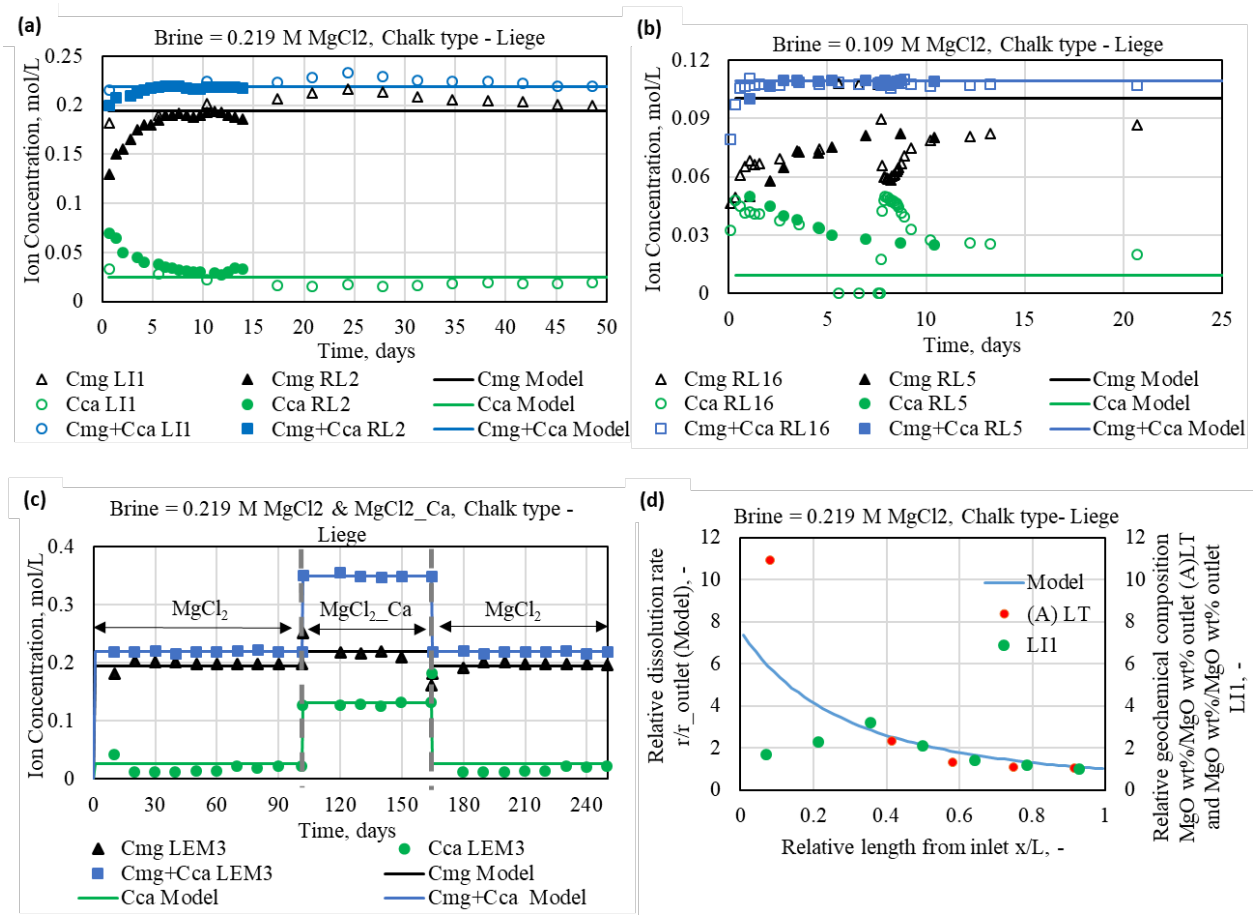

Figure 7 Simulated (analytical model) and experimental effluent concentrations of Ca, Mg and their sum during injection of 0.219 M $MgCl_2$ (Fig a), 0.109 M $MgCl_2$ (Fig b), alternation from 0.219 M $MgCl_2$ to 0.219 M $MgCl_2$ + 0.13 M $CaCl_2$ and then back to 0.219 M $MgCl_2$. In d; MgO wt% profiles measured along two cores after flooding 0.219 M $MgCl_2$ flooded for 516 d ((A)LT) and 65 d (LI1) compared with the steady state distribution of dissolution rate $\dot{r}$. Both scaled to outlet value.

The compaction model was then parameterized also for Liege, first by selection of m, k_{c0} from matching axial strain vs time for four tests with NaCl injection (**Figure 8a**). Then compaction data from cores injected with 0.109 and 0.219 M $MgCl_2$ were matched by assigning parameters k_c^{max} and $\dot{r}_{ref}$. Very similar compaction behavior was observed for these two concentrations in agreement with the similar production of Ca and retention of Mg in the effluent concentrations (~0.020 mol/L). The trends could indicate that lower values would be obtained with the low injected concentration if more time had passed. That would likely also result in less compaction with that brine as proposed by the match and prediction illustrated in **Figure 8b**.

In **Figure 8c** we see a test from Megawati et al. (2011) where various pH and Ca modified $MgCl_2$ brines were injected. pH effects are not accounted for in the model, but the effluent profiles in **Figure 7c** show same magnitude of Ca production and Mg retention the first ~100 d and last ~90 d. The first 100 d of compaction exhibit a variation of creep rate reduction and acceleration, triggered by the various brines. In this period, mainly the magnitude of compaction is captured as it was assumed only $MgCl_2$ was injected. At 100 d, when 0.13 M $CaCl_2$ + 0.219 M $MgCl_2$ was injected, inert rock-fluid behavior was observed and captured by the model. The switch of brine after 100 d results in a zero-dissolution rate which virtually stopped the compaction, see **Figure 8c**. On closer inspection compaction still occurs, but at very low rate.

This is understood from (43): After a significant period with reactive brine, the porosity has been reduced, yielding slower compaction than at higher porosities. Further, the compaction coefficient k_c is much lower at zero dissolution rate, see (58) and **Figure 2**. When $MgCl_2$ injection is restarted, the compaction rate coefficient increases again, and the solid volume reduction continues. The perturbation of chemistry on compaction is thus well captured.

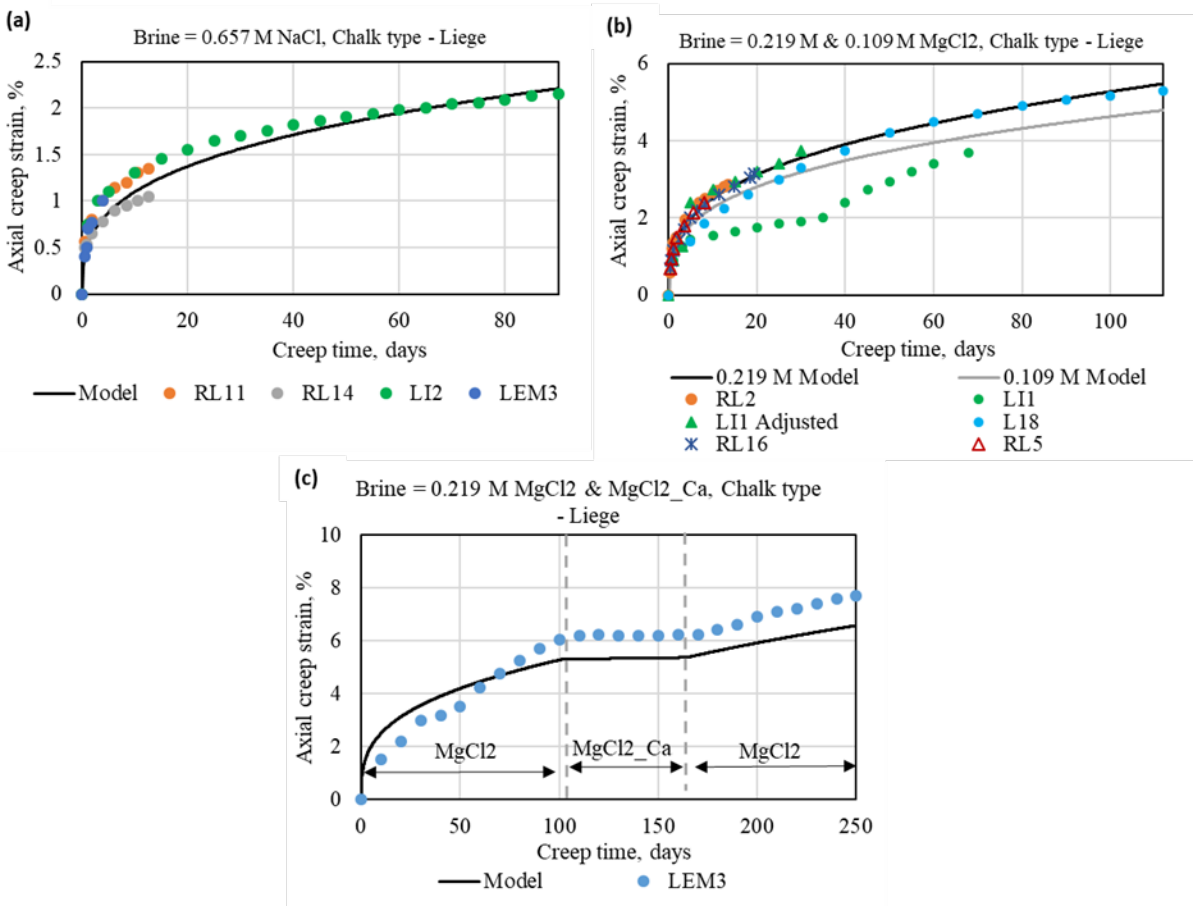

Figure 8 Comparison of creep compaction model with Liege cores injected at 1 PV/d with 0.657 M NaCl (left), 0.109 and 0.219 M $MgCl_2$ (right) and a test where pH and Ca modified 0.219 M $MgCl_2$ brines were injected.

Compaction Relation to Dissolution Rate

The relation between the compaction coefficient and dissolution rate is summarized for both chalks in **Figure 9**. It is seen that the sensitivity is very similar: small changes in reactiveness has a great impact on the compaction coefficient at low dissolution rates indicating that low reactive concentrations can greatly affect compaction behavior. At higher dissolution rates the sensitivity is less, and changes in the dissolution rate does not greatly affect the compaction rate further. The compaction coefficients the most reactive composition relative to with inert brine was a factor of 15 and 8 apart for Liege and Aalborg, respectively. This quantifies a significant contribution from water weakening to chemical compaction, i.e. reduction of volume due to replacing calcite with the smaller mineral magnesite does not alone explain the difference in compaction between tests with reactive and inert brines.

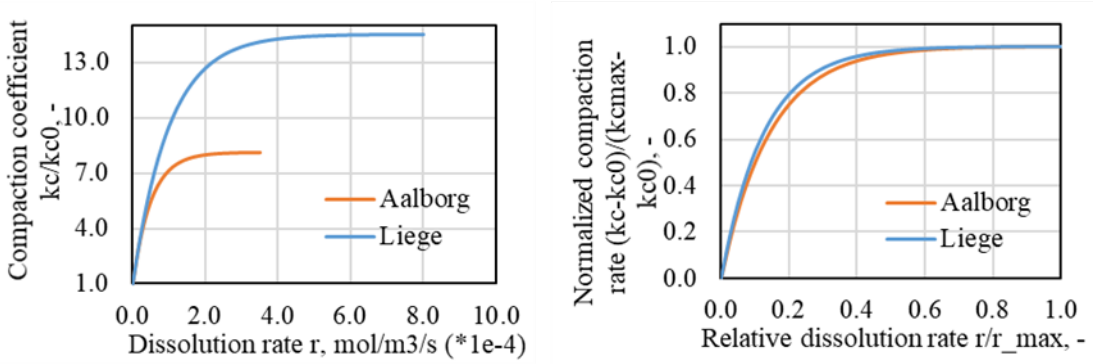

Figure 9 Compaction coefficient relation with dissolution rate obtained from interpretation of experiments. Absolute values (left) and scaled values (right).

Interpretation of a Long Term Test

The model was further applied to interpret a long term test of ~3 years where 0.219 M $MgCl_2$ was injected at 1 or 3 PV/d, see Nermoen et al. (2015). The effluent behavior is reasonably well matched, see **Figure 10a**. When increasing the injection rate, the brine gets lower residence time and reacts less with the rock. Thus, lower Ca^{2+} production and Mg^{2+} retention is seen with high rate (3 PV/d) compared to low rate (1 PV/d). Over time, a decreasing trend in Ca effluent concentrations is seen, especially after ~350 d. This may be due to a depletion in calcite mineral or less available reactive surface area for calcite dissolution which becomes important over large time scales. This was not built into the model and hence not accounted for.

The related creep compaction behavior is shown in **Figure 10b**. The model captures the sensitivity to changes in injection rate. At increased rate, the brine remains more reactive though the core. This results in a minor increase of the compaction rate at ~100 d when the injection rate goes from 1 to 3 PV/d. However, when the rate is switched back to 1 PV/d after 400 d, the model overestimates the compaction rate. This seems related to the discrepancy in effluent at late times. This leads to overestimation of solid volume reduction. Likely, it also means there is less accessible calcite structure and the predicted water weakening effects in the model no longer occur in the real core. Such effects could be built into the model by reducing the dissolution rate with a factor that would be 1 under conditions where calcite dominated the matrix composition and approach zero when the calcite content vanished, e.g. when $\frac{\rho_c}{\rho_c+\rho_m} \rightarrow 0$.

The deformation after the test is displayed in **Figure 10c** comparing the experimentally measured core diameter profile with the simulated. The length axis represents the compacted length in axial direction. As seen, the overestimation of compaction by the model has resulted in stronger reduction of axial and radial core dimensions. The simulated core length has been reduced from 7 to 5.8 cm and the core diameter has reduced from 3.8 to ~ 2.8 cm at the inlet and ~ 3.2 cm at the outlet which means 1/0.6 =1.7 times as much compaction at the inlet as the outlet. Note that the dissolution rate for 0.219 M $MgCl_2$ at 1 PV/d was modelled to 7.7 times higher in Liege at inlet vs the outlet. The relatively smaller impact on compaction is due to that compaction is not only controlled by chemistry, but also stress accommodation and that differences in dissolution rate do not give a proportional impact on compaction, see **Figure 9**. We will also show later that higher injection rates gives more uniform chemomechanical behavior.

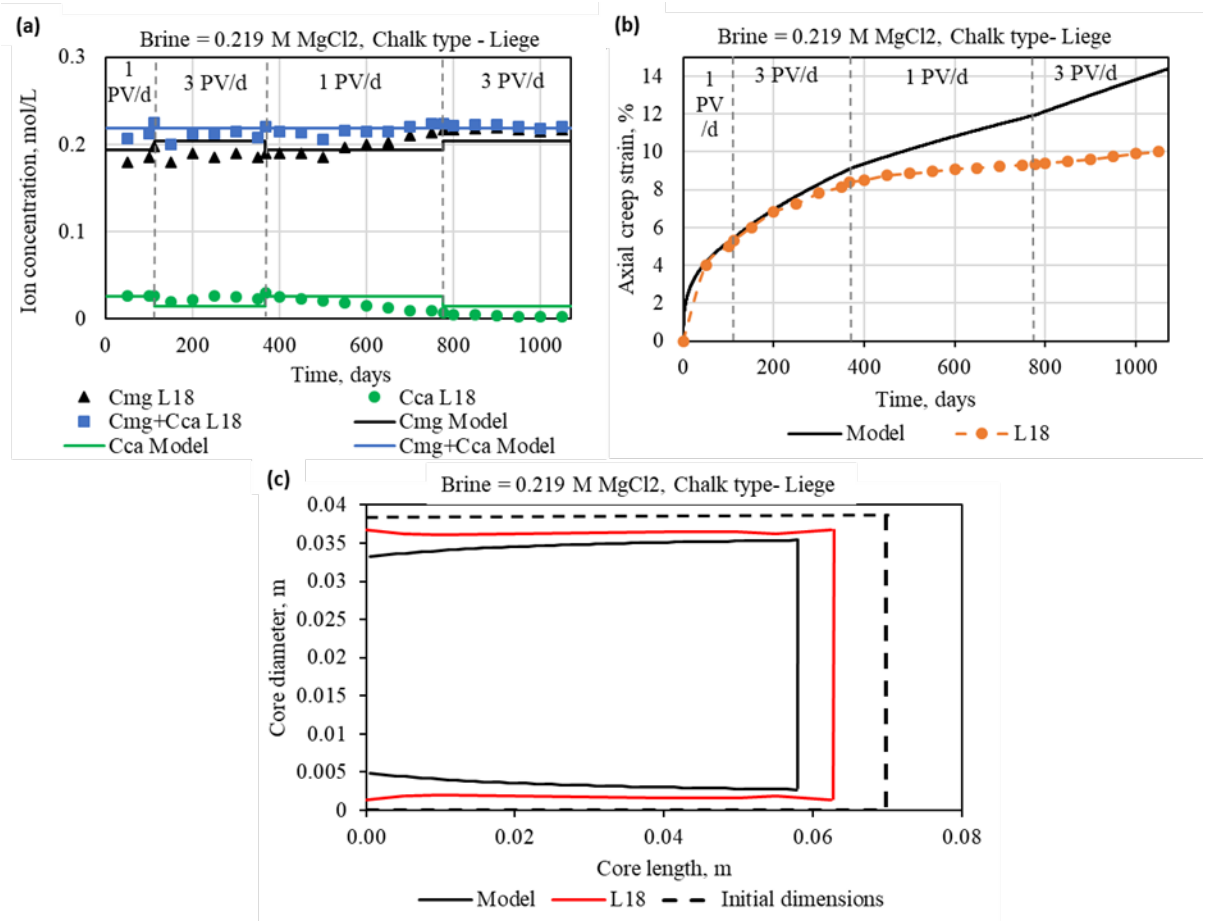

Figure 10 Data from a long term test ~3 years where 0.219 M $MgCl_2$ brine was flooded through a Liege chalk core (L18) at both 1 and 3 PV/d. Left: Simulated (predicted with analytical model) and experimental effluent concentrations of Ca and Mg and their sum. Right: simulated and observed creep compaction. Bottom: simulated (analytical model) and measured core dimensions after the test.

Variations of the Damköhler Number

In the following we vary injection rate systematically between 0.1 and 10 PV/d to understand the interplay in a core at different magnitudes of N_{Da} when reactive brine, represented by 0.219 M $MgCl_2$, is injected. Behavior for both chalk types is predicted.

A high injection rate gives the brine short residence time and leads to maintaining a highly reactive brine throughout the core, see **Figure 11**. The profiles of Ca concentration reduce and the dissolution rate increases with higher injection rate. At low injection rate 0.1 PV/d, strong precipitation of magnesite (and dissolution of calcite) is seen near the inlet compared to the remaining core, resulting in non-uniform mineral distributions. The spatial distribution of mineral concentrations becomes more uniform with increase in injection rate and the conversion of calcite into magnesite occurs to greater extent. The effect is seen the most further into the core. Particularly the dissolution rate is fixed to that given by the injected composition at $x = 0$.

This has some interesting implications when we compare the two chalk types. At 1 PV/d, the conditions where mineralogical profiles were measured; the reaction rate is much higher near the inlet than the outlet for Liege, while it is more uniform for Aalborg. The net effect on dissolution of calcite is however comparable since a similar concentration of 0.025 mol/L Ca is produced from the core in both cases (see e.g. **Figure 11a, e** at $\frac{x}{L} = 1$). Increasing the injection rate does not bring the dissolution rate along the core much higher in Aalborg (**Figure 11f**) since it is only ~0.8 times lower at the outlet to begin with. At higher injection rate this difference lessens giving comparable values to $\dot{r}(C_{inj})$ across the core. For Liege, the highly non-uniform distribution at 1 PV/d leads to a much greater increase in dissolution rate downstream when the rate is increased. Although the Ca effluent concentration reduces with higher

rate (due to lower residence time) we see (by close inspection) that at 10 PV/d it is ~0.06 mol/L for Liege and ~0.03 mol/L for Aalborg (seen at $\frac{x}{L} = 1$ in **Figure 11a, e**), i.e. at these conditions there is twice as much calcite dissolution in Liege as for Aalborg. This is reflected in the buildup of Mg mineral fraction where after 320 d the average Mg mineral fraction is ~0.55, while it is 0.3 for Aalborg. At low rate 0.1 PV/d the high residence time causes the brine to lose reactivity in short distance. This is most pronounced for Liege which obtains three times lower effluent concentration of Ca than for Aalborg (0.037 mol/L and 0.105 mol/L) and thus three times lower Mg mineral precipitation as for Aalborg (**Figure 11d, h**).

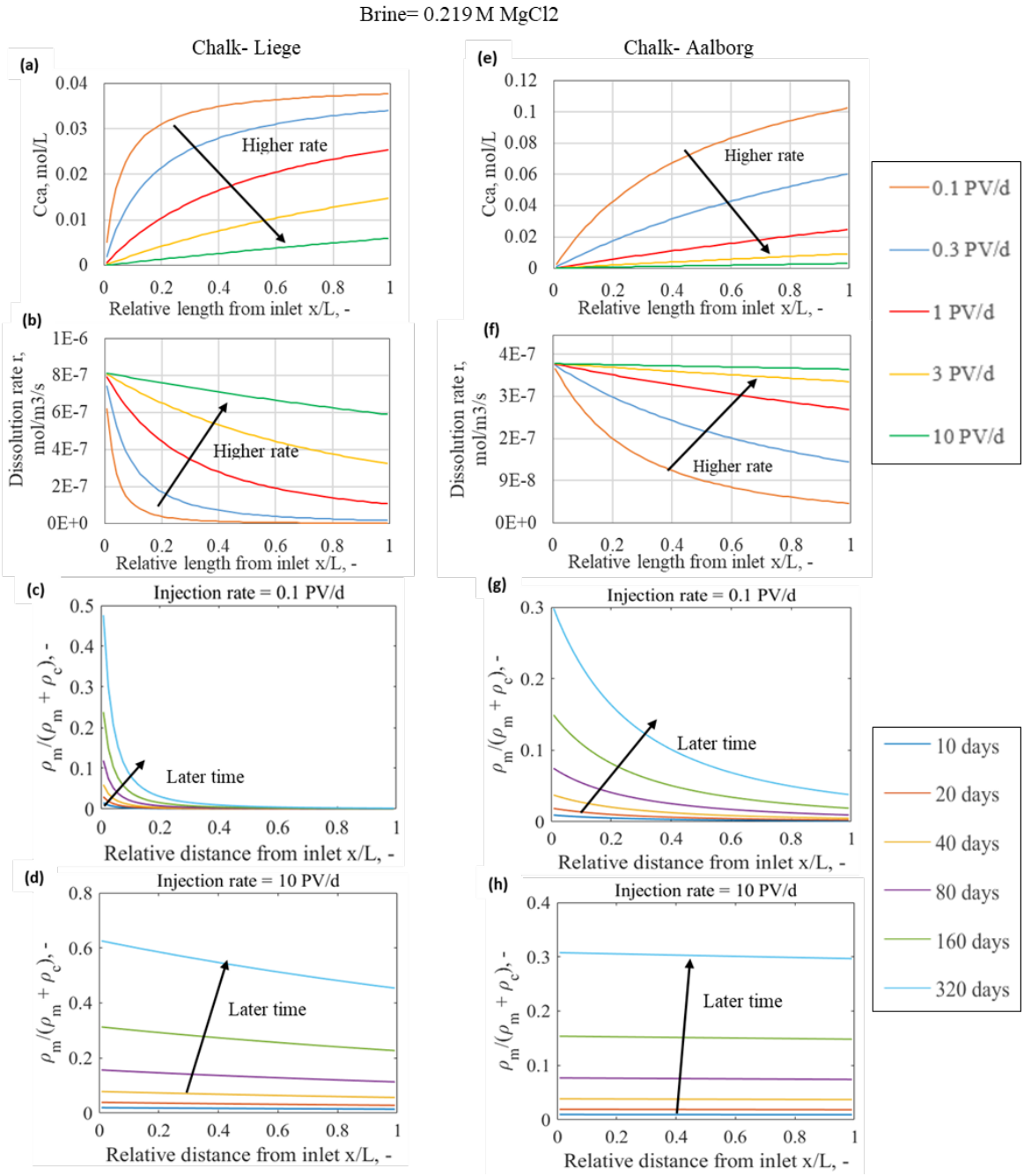

Figure 11 Simulated (analytical model) steady state distribution of Ca concentration (a) and dissolution rate (b) at different injection rates. Magnesite mineral fraction distribution with time for low (c) and high injection rate (d) for Liege data when 0.219 M $MgCl_2$ is injected at various constant injection rates. The same for Aalborg in (e) to (h).

Figure 12 shows that the axial strain and porosity vs time for the cases previously demonstrated. It is seen for both chalks that a higher injection rate leads to greater compaction and reduced porosity. Liege was shown to change most regarding the dissolution rate along the core with rate and thus is highly sensitive

to rate in terms of compaction and porosity. Aalborg, which demonstrated similar magnitude of dissolution rate unless the injection rate was lowered, also showed little sensitivity in compaction to increases in injection rate, while the low injection rate case (0.1 PV/d) stood out the most from the rest with less compaction. The non-uniform reaction rate distributions associated with low injection rates also resulted in non-uniform compaction along the core with the inlet diameter of Liege compacting by a factor ~0.9 and the outlet diameter by a factor ~0.96 after 320 d. For Aalborg the overall compaction was higher, but the difference between inlet compaction (0.88) and the outlet (0.91) was less. For this case the Liege core compacts half as much as Aalborg (4.5 % vs 9 % axial strain after 320 d). At high injection rate (10 PV/d) both cores compact more uniformly and more, due to the higher dissolution rate. The effect is most pronounced for Liege which after 320 d has compacted very comparably with Aalborg (~9.8 % and ~10.5 % axial strain, respectively, see **Figure 12a, e**).

We thus identify essentially two reaction-compaction regimes. High injection rate gives a relatively uniform and high dissolution rate with corresponding uniform and high compaction rate. In the low rate case, non-uniform and low dissolution rate along the core results in non-uniform, and generally less compaction.

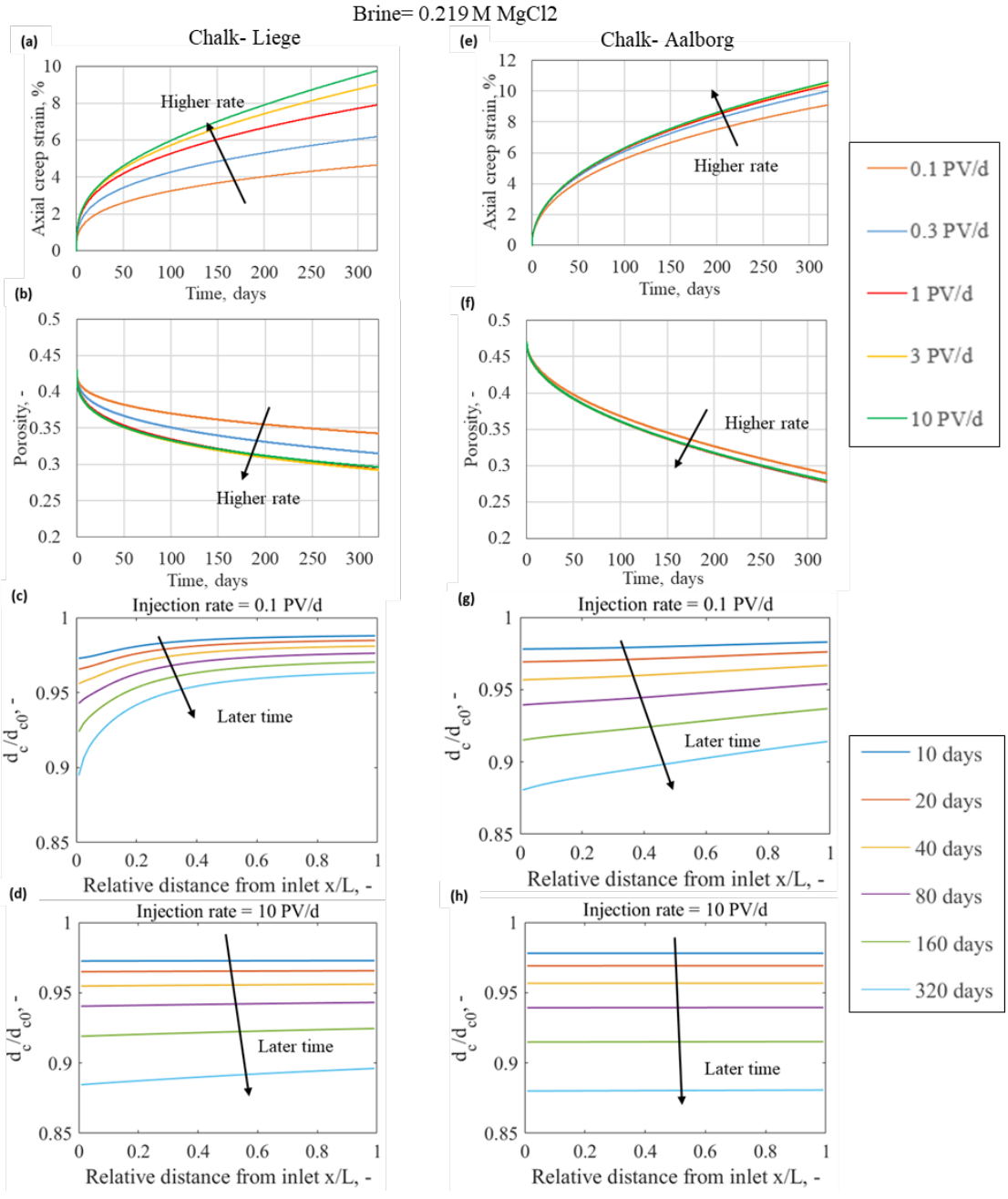

Figure 12 Simulated (analytical model) axial strain vs time (a), porosity vs time (b), radial compaction profile along the core for different times at low rate (c) and high rate (d) for Liege data when 0.219 M $MgCl_2$ is injected at various constant injection rates. The same is shown for Aalborg data in (e) to (h).

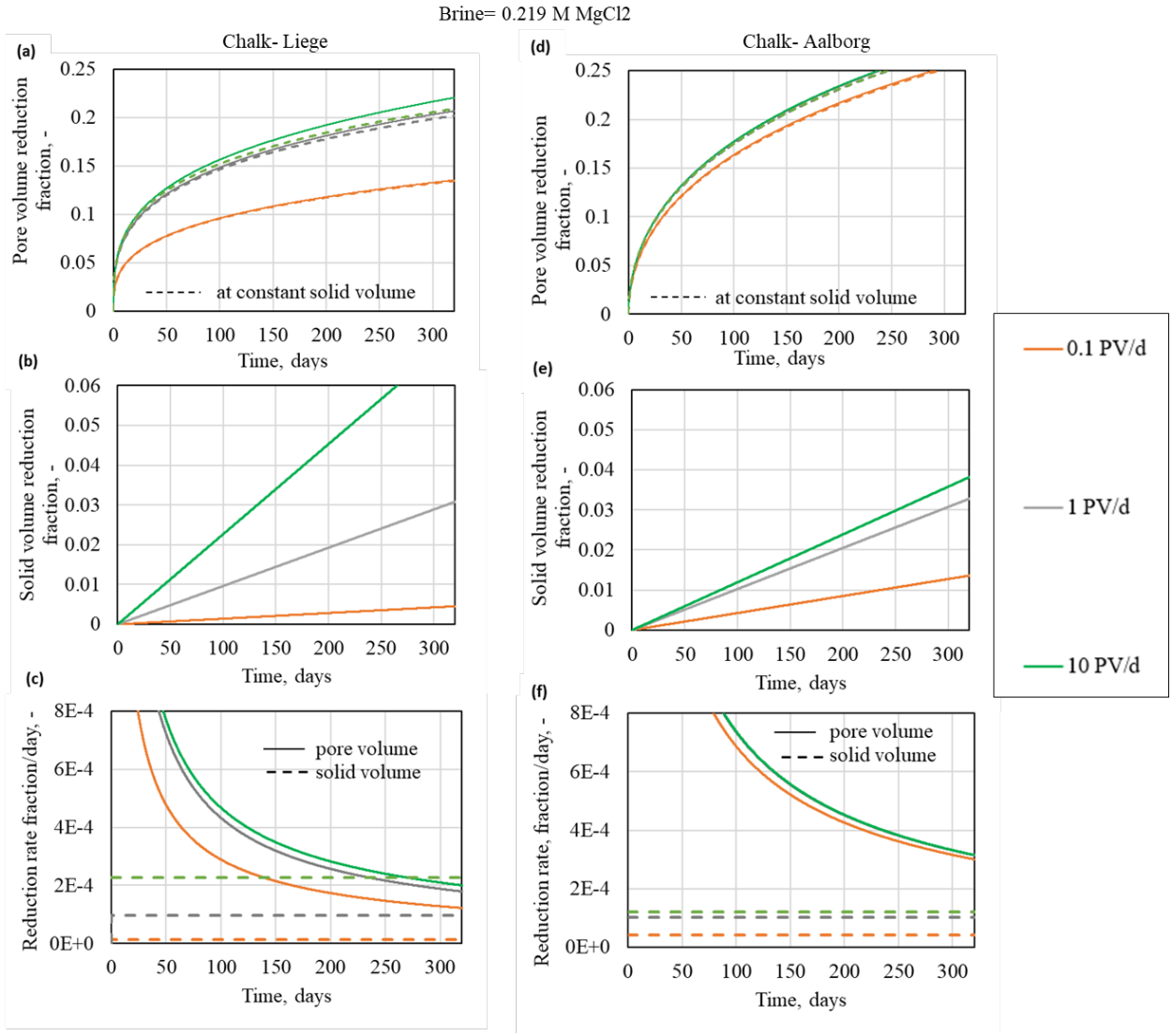

Figure 13 Simulated (analytical model) pore volume reduction (a) and solid volume reduction (b), for Liege both relative to the original bulk volume. Also, the rate change of these fractions (c). The same for Aalborg in (d) to (f). 0.219 M $MgCl_2$ brine is injected at various constant injection rates.

The contributions to compaction from reductions in pore volume and solid volume are investigated for injection of 0.219 M $MgCl_2$ at 0.1, 1 and 10 PV/d. Relative pore volume reduction (V_{p_r}) and relative solid volume reduction (V_{s_r}) are plotted in **Figure 13** and are defined as the change in pore volume and solid volume relative to the initial bulk volume V_0:

$$V_{p_r}(t) = \frac{V_{p0} - V_p(t)}{V_0}, \tag{70}$$

$$V_{s_r}(t) = \frac{V_{s0} - V_s(t)}{V_0}, \tag{71}$$

where V_{p0} and V_{s0} are initial pore and solid volume of the core, respectively. A sharp pore volume reduction is seen at early times for all injection rates and both chalks. Compared with solid volume the reduction of pore volume is the main contributor to compaction during the considered time period of 320 d. However, the rate of pore volume reduction drops significantly with time whereas the solid volume reduction rate remains constant. For Liege the contributions to compaction are thus comparable at late

times, especially for injection rate of 10 PV/d where the reduction of solid volume is dominant after 270 d. Although changes in solid volume affect porosity and hence the stress accommodation mechanism, the impact of keeping the solid volume constant appears negligible as seen in **Figure 13a, d**.

Change of Brine Composition

In **Figure 14** the role of changing concentration of injected $MgCl_2$ brine is considered, from 0.219 M down to 0 M. Lowering the injected concentration makes the inlet composition less reactive, however, since $C_{ca}^{inj} = 0$, the brine is always reactive and will predict dissolution of calcite and precipitation of magnesite except for the 0 M $MgCl_2$ case.

The dissolution rate falls rapidly when the concentration is lowered (halved at every interval) due the reaction order of $n = 2$. The corresponding impact on compaction is more gradual for both chalks with similar intervals between the compaction curves.

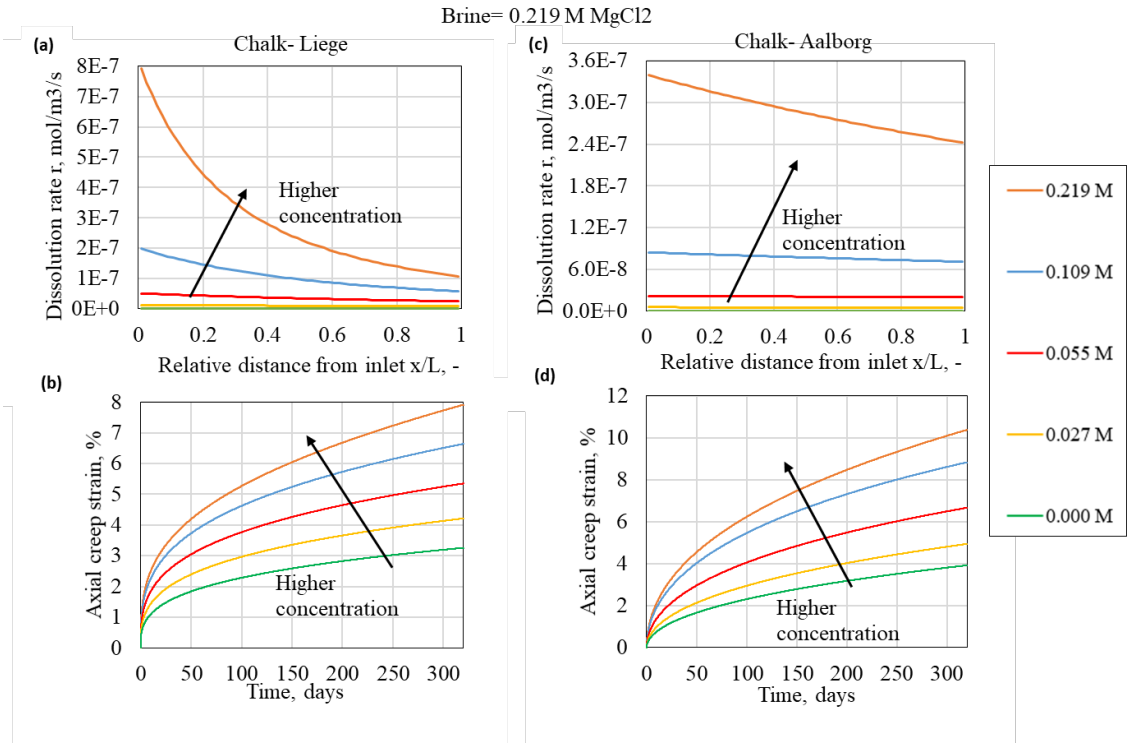

Figure 14 Simulated (analytical model) distribution of dissolution rate (a) and axial creep (b) when $MgCl_2$ of different concentrations are injected at 1 PV/d in Liege chalk. The same for Aalborg in (c) and (d).

As demonstrated previously, see **Figure 7**, injecting an inert brine could delay compaction rate. We now wish to see if this holds true under more general conditions. Using Liege and Aalborg data; 0.219 M $MgCl_2$ is injected at constant rate (0.1 or 10 PV/d). After an indicated period of time (10, 20, to 320 d), the injection brine is switched to inert composition for 50 d, before switching back to 0.219 M $MgCl_2$. As seen in **Figure 15**, at low injection rate, switching to inert brine reduces, but does not stop, the compaction rate. At low injection rate the overall dissolution rate is low. Chemistry has less impact on changing the solid volume and the compaction coefficient. At high injection rate, a high dissolution rate occurs along the entire core with impacts on both solid volume and the compaction coefficient. This gives a high compaction rate at a given time and switching to inert brine the compaction rate becomes low in comparison. Interestingly, regardless of injection rate and chalk type; no matter when the inert brine is injected the axial compaction profile appears to continue along the same path after switching back to $MgCl_2$ after the considered period (50 d) of slow compaction.

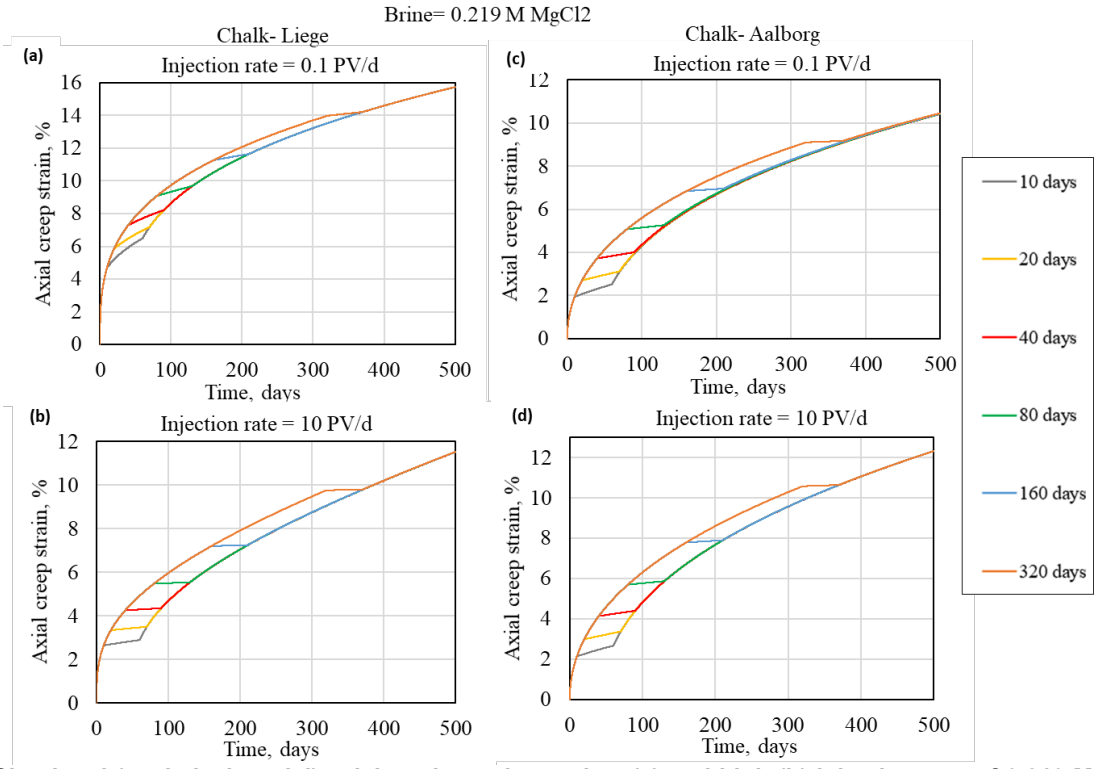

Figure 15 Simulated (analytical model) axial strain vs time at low (a) and high (b) injection rate of 0.219 M $MgCl_2$ into Liege chalk for the indicated period of time, then injecting 0.657 M NaCl for 50 d (at the indicated time) and then return to injecting 0.219 M $MgCl_2$. The same for Aalborg chalk in (c) and (d).

Evaluation of Model Assumptions

The system we have considered has assumed a reaction kinetics which is of a substitution-like form. That is indeed representative for the Ca-Mg-Na-Cl-brine and chalk system, but implied that the changes in solid volume are negligible compared to the changes in pore volume in terms of compaction although dramatic chemical alterations of the rock and strong chemical compaction are seen. Brines containing ions such as sulfate (seawater) can lead to excess precipitation (Madland et al. 2011) and hence permeability reduction. The same can be seen if reactive in-situ non-carbonate minerals are present such as opal-CT (Andersen et al. 2018; Minde et al. 2018). This would give solid volume changes a greater contribution.

The reaction kinetics along the core were based on instantaneously establishing steady state according to the injected rate and composition. It really requires at least one pore volume to displace the previous fluid and dispersion and surface mechanisms can cause further delays. Since the tests we considered were applying 10's or 100's of PVs and the transient solution quickly is comparable with steady state, the transition was not considered to play a great role. Depending on whether the change in injection conditions favors uptake of Mg over Ca or opposite will also determine whether the transient phase will provide higher or lower dissolution rate along the core compared to the steady state solution. As an example; Injection of MgCl2 into a system with only Ca on the surface will induce adsortion of Mg and release of Ca ions, which makes the brine less reactive compared to the steady state.

Reduction of the porous area with compaction will tend to increase the interstitial velocity which gives local and time dependent changes in N_{Da}. By the given approach we preserve the volume of fluid injected and interacting with the rock, but may overestimate the residence time. Similarly, changes in specific surface area or mineral coverage can affect the reaction rate. The main goal of the work is to quantify the link between compaction and reaction in a transparent way. For short term tests and improved consistency with observed behavior it is recommended to use the transient solution and obtain detailed information about the stated relations for input in simulations.

Conclusions

In this work we have presented a mathematical model to describe the interaction between reactive flow

and creep compaction in chalk for interpretation of core flooding-compaction tests under uniform stress conditions. For given injection rate and injected composition, the ion and dissolution rate profiles were calculated analytically using a steady state assumption. The creep compaction was related to three mechanisms: 1) pore volume reduction by stress accommodation. This is driven by effective stress and resisted by reduction of porosity; 2) Solid volume reduction due to dissolution of calcite which is replaced on molar basis by the smaller mineral magnesite, directly linked to the dissolution rate; 3) Chemical weakening, coupling the two mechanisms where higher dissolution rate enhanced the pore volume reduction by stress accommodation. The model was parameterized in terms of chemistry, compaction and their relating mechanisms by matching and interpreting effluent, geochemistry and compaction data from 22 core flooding tests where reactive or inert Mg-Ca-Na-Cl brines were injected. The model accounts for changes in injection rate, brine composition, applied stresses (external and pore) and temperature and could predict the corresponding impact on effluent concentrations, distributions of axial and radial compaction, porosity and mineral concentrations. The main conclusions are:

- The Aalborg chalk's chemical interaction with $MgCl_2$ brine could be interpreted by thermodynamically predicted equilibrium states and literature measured reaction order for magnesite precipitation. That was not possible for Liege chalk in which stable oversaturation was a possible explanation required to explain the combined observations.
- The considered reactive brines give a net solid volume reduction when calcite dissolves and magnesite precipitates. However, the enhanced compaction during injection of these reactive brines is strongly dominated by enhanced pore volume reduction (the chemical weakening mechanism) and only at late times (after months) the solid volume.
- The relation between chemical weakening and dissolution rate was quantified. For both chalk types it was found that enhanced compaction occurs is sensitive to even weak chemical interactions. At stronger dissolution rates the sensitivity to increased dissolution rate is less.
- In line with experimental observations, the model could predict non-uniform compaction related to the locations affected by chemistry. At high N_{Da} strong interaction occurs with the brine so it loses reactivity. The non-uniform dissolution rate results in non-uniform compaction. At low N_{Da} the brine interacts weakly with the rock and maintains a high dissolution rate along the entire core with resulting uniform compaction.
- Switching from a reactive to an inert brine can appear to stop compaction (Megawati et al. 2011). Our model could reproduce this behavior, but suggests that this would not be the case at low injection rate or if the switch occurred at low strain (early time). In reactive systems with high injection rate, switching to inert brine at a high strain induces negligible compaction rate. The axial compaction profiles always continued along the same profile after switching back to reactive brine from inert brine, irrespective of injection rate and the time inert brine was injected.
- The model predicts that at injection of 0.219 M $MgCl_2$ at low injection rate (0.1 PV/d) Aalborg chalk will dissolve ~3x more calcite than Liege chalk, while at high injection rate (10 PV/d) Aalborg will dissolve ~2x less calcite than Liege chalk.
- The model predicts that Liege chalk will respond strongly in compaction to changes in injection rate, while Aalborg chalk will show little response. Both chalks will respond strongly to changes in the injected brine concentration.

The predictions in the last three points are recommended to test experimentally in future work. The model was derived and demonstrated for systems that are well studied by systematic experimental investigations. More complex rock-brine systems are relevant such as by adding sulfate and anhydrite minerals to the model for better representation of seawater-like brines. Alterations of the mineralogy could affect the reaction kinetics, especially in long term tests where calcite is exhausted or the available surface area for reactions changes. We further note that the model is not limited to assuming the steady state solution. Solving the full transient model with compaction would give gradual changes in the dissolution rate distribution with resulting gradual impact on the compaction rate. In this first presentation of the model we have focused on the steady state between advection and reaction since that allows direct coupling of explicit solutions to interpret compaction behavior. The model also naturally extends to include

multiphase flow. In all cases, relevant experimental data should be considered to parameterize the model.

Acknowledgments

The authors acknowledge the Research Council of Norway and the industry partners, ConocoPhillips Skandinavia AS, Aker BP ASA, Vår Energi AS, Equinor ASA, Neptune Energy Norge AS, Lundin Norway AS, Halliburton AS, Schlumberger Norge AS, Wintershall Norge AS, and DEA Norge AS, of The National IOR Centre of Norway for support.

References

1. Akin, S., Schembre, J. M., Bhat, S. K., & Kovscek, A. R. (2000). Spontaneous imbibition characteristics of diatomite. *Journal of Petroleum Science and Engineering*, **25**(3-4), 149-165.
2. Andersen, M. A., Foged, N., & Pedersen, H. E. (1992). The rate-type compaction of a weak North Sea chalk. In *The 33th US Symposium on Rock Mechanics (USRMS)*.
3. Andersen, P. Ø., Evje, S., Madland, M. V., & Hiorth, A. (2012). A Geochemical Model for Interpretation of Chalk Core Flooding Experiments. *Chemical Engineering Science*, **84**, 218-241. https://doi.org/10.1016/j.ces.2012.08.038
4. Andersen, P. Ø., Evje, S., Kleppe, H., & Skjaeveland, S. M. (2015). A Model for Wettability Alteration in Fractured Reservoirs. *SPE Journal*, **20**(6), 1-261. https://doi.org/10.2118/174555-PA
5. Andersen, P. Ø., & Evje, S. (2016). A Model for Reactive Flow in Fractured Porous Media. *Chemical Engineering Science*, **145**, 196-213, https://doi.org/10.1016/j.ces.2016.02.008
6. Andersen, P. Ø., Wang, W., Madland, M. V., Zimmermann, U., Korsnes, R. I., Bertolino, S. R. A., Minde, M. W., Schulz, B., & Gilbricht, S. (2018). Comparative Study of Five Outcrop Chalks Flooded at Reservoir Conditions: Chemo-mechanical Behaviour and Profiles of Compositional Alteration. *Transport in Porous Media*, **121**(1), 135-181. https://doi.org/10.1007/s11242-017-0953-6
7. Appelo, C. A. J., & Postma, D. (2004). *Geochemistry, groundwater and pollution*. CRC press.
8. Austad, T., Strand, S., Madland, M. V., Puntervold, T., & Korsnes, R. I. (2008). Seawater in Chalk: An EOR and Compaction Fluid. *SPE Reservoir Evaluation & Engineering*, **11**(4), 648-654. https://doi.org/10.2118/118431-PA
9. Barenblatt, G. I., & Prostokishin, V. M. (1993). A mathematical model of damage accumulation taking into account microstructural effects. *European Journal of Applied Mathematics*, **4**(3), 225-240. https://doi.org/10.1017/S0956792500001108
10. Cristescu, N. (1994). A procedure to determine nonassociated constitutive equations for geomaterials. *International Journal of Plasticity*, **10**(2), 103-131. https://doi.org/10.1016/0749-6419(94)90031-0
11. Cuiec, L., Bourbiaux, B., & Kalaydjian, F. (1994). Oil recovery by imbibition in low-permeability chalk. *SPE Formation Evaluation*, *9*(3), 200-208.
12. Dahou, A., Shao, J. F., & Bederiat, M. (1995). Experimental and numerical investigations on transient creep of porous chalk. *Mechanics of materials*, **21**(2), 147-158. https://doi.org/10.1016/0167-6636(95)00004-6
13. Evje, S., Hiorth, A., Madland, M. V., & Korsnes, R. I. (2009). A mathematical model relevant for weakening of chalk reservoirs due to chemical reactions. *NHM*, **4**(4), 755-788. http://dx.doi.org/10.3934/nhm.2009.4.755
14. Fjær, E., Horsrud, P., Raaen, A. M., Risnes, R., & Holt, R. M. (1992). *Petroleum related rock mechanics* (Vol. 33). Elsevier.
15. Fogler, S. (2006). *Elements of Chemical Reaction Engineering* (4th ed.). Upper Saddle River, NJ: Pearson Education.
16. Graue, A., Viksund, B. G., Baldwin, B. A., & Spinler, E. A. (1999). Large-Scale Two-Dimensional Imaging of Wettability Effects on Fluid Movement and Oil Recovery in Fractured Chalk. *SPE Journal*, **4**(1), 25-36. http://dx.doi.org/10.2118/54668-PA
17. Hellmann, R., Renders, P. J., Gratier, J. P., & Guiguet, R. (2002). Experimental pressure solution

compaction of chalk in aqueous solutions. Part 1. Deformation behavior and chemistry. *Water-rock interactions, ore deposits, and environmental geochemistry: A tribute to David A. Crerar*, *7*, 129-152.
18. Hirasaki, G., & Zhang, D. L. (2004). Surface chemistry of oil recovery from fractured, oil-wet, carbonate formations. *SPE Journal*, **9**(2), 151-162. https://doi.org/10.2118/88365-PA
19. Hjuler, M. L. (2007). Diagenesis of Upper Cretaceous onshore and offshore chalk from the North Sea area (PhD Dissertation). *Institute of Environment & Resources*.
20. Jaeger, J. C., & Cook, N. G. W. (1976). *Fundamentals of Rock Mechanics* (No. SP18 Monograph).
21. Kee, R. J., Coltrin, M. E., & Glarborg, P. (2005). *Chemically reacting flow: theory and practice*. John Wiley & Sons.
22. Kharaka, Y. K., Cole, D. R., Hovorka, S. D., Gunter, W. D., Knauss, K. G., & Freifeld, B. M. (2006). Gas-water-rock interactions in Frio Formation following CO2 injection: Implications for the storage of greenhouse gases in sedimentary basins. *Geology*, **34**(7), 577-580. https://doi.org/10.1130/G22357.1
23. Land, L. S. (1998). Failure to Precipitate Dolomite at 25 C fromDilute Solution Despite 1000-Fold Oversaturation after32 Years. *Aquatic Geochemistry*, *4*(3), 361-368.
24. Langmuir, D. (1997). *Aqueous environmental geochemistry*. Prentice Hall.
25. Logan, J. D. (2013). *Transport modeling in hydrogeochemical systems* (Vol. 15). Springer Science & Business Media.
26. Korsnes, R. I., Strand, S., Hoff, Ø., Pedersen, T., Madland, M. V., & Austad, T. (2006). Does the chemical interaction between seawater and chalk affect the mechanical properties of chalk. In *Eurock* (pp. 427-434).
27. Madland, M. V., Hiorth, A., Omdal, E., Megawati, M., Hildebrand-Habel, T., Korsnes, R. I., Evje, S. & Cathles, L. M. (2011). Chemical alterations induced by rock–fluid interactions when injecting brines in high porosity chalks. *Transport in Porous Media*, **87**(3), 679-702. https://doi.org/10.1007/s11242-010-9708-3
28. Megawati, M., Andersen, P. Ø., Korsnes, R. I., Evje, S., Hiorth, A., & Madland, M. V. (2011). The Effect of Aqueous Chemistry pH on the Time-Dependent Deformation Behaviour of Chalk - Experimental and Modelling Study. In *Pore2Fluid IFP Energies nouvelles Paris, Nov*, 16-18.
29. Megawati, M., Madland, M. V., & Hiorth, A. (2015). Mechanical and physical behavior of high-porosity chalks exposed to chemical perturbation. *Journal of Petroleum Science and Engineering*, **133**, 313-327. https://doi.org/10.1016/j.petrol.2015.06.026
30. Minde, M. W., Wang, W., Madland, M. V., Zimmermann, U., Korsnes, R. I., Bertolino, S. R. A., & Andersen, P. Ø. (2018). Temperature Effects on Rock Engineering Properties and Rock-Fluid Chemistry in Opal-CT-Bearing Chalk. *Journal of Petroleum Science and Engineering,* **169**, 454-470. https://doi.org/10.1016/j.petrol.2018.05.072
31. Morrow, N. R., & Mason, G. (2001). Recovery of oil by spontaneous imbibition. *Current Opinion in Colloid & Interface Science*, **6**(4), 321-337. https://doi.org/10.1016/S1359-0294(01)00100-5
32. Nermoen, A., Korsnes, R. I., Hiorth, A., & Madland, M. V. (2015). Porosity and permeability development in compacting chalks during flooding of nonequilibrium brines: Insights from long-term experiment. *Journal of Geophysical Research: Solid Earth*, **120**(5), 2935-2960. https://doi.org/10.1002/2014JB011631
33. Nermoen, A., Korsnes, R. I., Aursjø, O., Madland, M. V., Kjørslevik, T. A., & Østensen, G. (2016). How stress and temperature conditions affect rock-fluid chemistry and mechanical deformation. *Frontiers in Physics*, **4**, 2. https://doi.org/10.3389/fphy.2016.00002
34. Parkhurst, D. L., & Appelo, C. A. J. (2013). *Description of input and examples for PHREEQC version 3: a computer program for speciation, batch-reaction, one-dimensional transport, and inverse geochemical calculations* (No. 6-A43). US Geological Survey.
35. Ruddy, I., Andersen, M. A., Pattillo, P. D., Bishlawi, M., & Foged, N. (1989). Rock compressibility, compaction, and subsidence in a high-porosity chalk reservoir: A case study of Valhall field. *Journal of Petroleum Technology*, **41**(7), 741-746. https://doi.org/10.2118/18278-

PA
36. Saldi, G. D., Jordan, G., Schott, J., & Oelkers, E. H. (2009). Magnesite growth rates as a function of temperature and saturation state. *Geochimica et Cosmochimica Acta*, *73*(19), 5646-5657.
37. Shinn, E. A., & Robbin, D. M. (1983). Mechanical and chemical compaction in fine-grained shallow-water limestones. *Journal of Sedimentary Research*, **53**(2), 595-618. https://doi.org/10.1306/212F8242-2B24-11D7-8648000102C1865D
38. Sylte, J. E., Thomas, L. K., Rhett, D. W., Bruning, D. D., & Nagel, N. B. (1999). Water induced compaction in the Ekofisk field. In *SPE Annual Technical Conference and Exhibition*. https://doi.org/10.2118/56426-MS
39. Zhang, P., Tweheyo, M. T., & Austad, T. (2007). Wettability alteration and improved oil recovery by spontaneous imbibition of seawater into chalk: Impact of the potential determining ions Ca2+, Mg2+, and SO42−. *Colloids and Surfaces A: Physicochemical and Engineering Aspects*, **301**(1-3), 199-208. https://doi.org/10.1016/j.colsurfa.2006.12.058
40. Zimmermann, U., Madland, M. V., Nermoen, A., Hildebrand-Habel, T., Bertolino, S. A., Hiorth, A., Korsnes, R. I., Audinot, J. & Grysan, P. (2015). Evaluation of the compositional changes during flooding of reactive fluids using scanning electron microscopy, nano-secondary ion mass spectrometry, x-ray diffraction, and whole-rock geochemistry. *AAPG Bulletin*, **99**(5), 791-805. https://doi.org/10.1306/12221412196

Appendix

A) Equilibrium concentrations

Theoretical equilibrium conditions were evaluated with Phreeqc v3 (Parkhurst & Appelo 2013). Ca-Mg-Na-Cl brine compositions were allowed to equilibrate by dissolving calcite and precipitating magnesite. Results for diluted $MgCl_2$ brines are shown in **Table 5** and results for 0.219 M $MgCl_2$ with additions of $CaCl_2$ are shown in **Table 6**. The original brine composition and ionic strength are indicated together with the equilbrium concentrations of Ca and Mg, the ratio of total concentration of Ca and Mg after and before equilibration, as well as the ratio of equilibrium concentration Mg to Ca ($k_2 = \frac{C_{mg}^{eq}}{C_{ca}^{eq}}$). The former ratio is ≈ 1 indicating that substitution is a very good assumption. The latter ratio is almost identical between all cases to 0.39. In this way a base value of $k_2 = 0.39$ was selected at 130° C. 0.219 M MgCl2 was equilibrated for different temperatures, see **Table 7**. Substitution behavior was still predicted, although the values of $k_2 = \frac{C_{mg}^{eq}}{C_{ca}^{eq}}$ indicated a strong temperature dependence with higher values at lower temperature (2.35 at 25° C).

Table 5 $MgCl_2$ brines equilibrated with calcite and magnesite at 130 °C using Phreeqc.

Conc of $MgCl_2$ (M)	I (-)	C_{ca}^{eq} (M)	C_{mg}^{eq} (M)	$\frac{C_{ca}^{eq}+C_{mg}^{eq}}{C_{ca}^{0}+C_{mg}^{0}}$ (-)	$\frac{C_{mg}^{eq}}{C_{ca}^{eq}}$ (-)
0.050	0.15	0.036	0.014	1.002	0.40
0.109	0.33	0.078	0.031	1.000	0.39
0.150	0.45	0.108	0.042	0.999	0.39
0.219	0.66	0.158	0.061	1.000	0.39
0.250	0.75	0.180	0.070	0.999	0.39

Table 6 0.219 M $MgCl_2$ with additions of $CaCl_2$ equilibrated with calcite and magnesite at 130 °C using Phreeqc.

Conc of $CaCl_2$ (M)	I (-)	C_{ca}^{eq} (M)	C_{mg}^{eq} (M)	$\frac{C_{ca}^{eq}+C_{mg}^{eq}}{C_{ca}^{0}+C_{mg}^{0}}$ (-)	$\frac{C_{mg}^{eq}}{C_{ca}^{eq}}$ (-)
0.050	0.81	0.195	0.074	1.000	0.38
0.100	0.96	0.232	0.087	1.000	0.38
0.130	1.05	0.251	0.098	1.000	0.39
0.150	1.11	0.265	0.104	1.000	0.39

Table 7 0.219 M $MgCl_2$ equilibrated with calcite and magnesite at different temperature using Phreeqc.

Temper-ature ($^{\circ}C$)	I (-)	C_{ca}^{eq} (M)	C_{mg}^{eq} (M)	$\frac{C_{ca}^{eq}+C_{mg}^{eq}}{C_{ca}^{0}+C_{mg}^{0}}$ (-)	$\frac{C_{mg}^{eq}}{C_{ca}^{eq}}$ (-)
130	0.219	0.158	0.061	1.000	0.39
110	0.219	0.148	0.072	1.000	0.49
90	0.219	0.134	0.085	1.000	0.64
60	0.219	0.106	0.113	1.000	1.07
40	0.219	0.083	0.136	1.000	1.63
25	0.219	0.065	0.154	1.000	2.35

B) Solving the Reactive Flow Model

The general model (3) is scaled using:

$$x' = \frac{x}{L}, \qquad t' = \frac{t}{\tau}, \qquad D' = \frac{D}{\left(\frac{L^2}{\tau}\right)}. \tag{72}$$

where τ is a reference time scale set to 1 day. Define $q = \frac{t_{ref} v_w}{\tau}$ as the number of PVs injected per day giving:

$$\partial_{t'}(C_i + \beta_i CEC) = -q\partial_{x'}C_i + D'\partial_{x'x'}C_i + \tau\,\dot{r}_i, \tag{73}$$

$$\partial_{t'}\rho_i = \tau\,\dot{r}_i. \tag{74}$$

The equations are then solved using an operator splitting approach:

1) Advection and dispersion transport is solved using an explicit second order numerical scheme.
2) Reaction transport is solved separately using the Matlab routine ode23tb.
3) Ion exchange is performed by updating the distribution of species between surface and brine at every splitting step.

More details on this procedure can be found in Andersen et al. (2012; 2015).